In Silico Docking of Rhodanine Derivatives and 3D-QSAR Study to Identify Potent Prostate Cancer Inhibitors

Koffi Alexis Respect Kouassi[1], Adenidji Ganiyou[2*], Diomande Gbe Gondo Didier[2], Anoubilé Benié[1,3], Ziao Nahossé[1]

[1]Laboratoire de Thermodynamique et de Physico-Chimie du Milieu, UFR SFA, Université Nangui Abrogoua, Abidjan, Côte d'Ivoire

[2]Laboratoire de Constitution et de Réaction de la matière, UFR-SSMT, Université Félix Houphouët-Boigny, Abidjan, Côte d'Ivoire

[3]Laboratoire de Chimie Bio-Organique et de Substances Naturelles, UFR-SFA, Université Nangui Abrogoua, Abidjan, Côte-d'Ivoire

Email: *adeganiyou@gmail.com

Abstract

The 3VHE protein is considered as a potential target for the treatment of prostate cancer. In order to find new 3VHE inhibitors, pharmacophore models based on the molecular structure of rhodanine derivatives and a three-dimensional quantitative structure-activity relationship model (3D-QSAR) have been developed and validated by different methods. The 3D-QSAR model was evaluated for its predictive performance on a diverse test set containing 18 prostate cancer inhibitors. It presents very interesting internal and external statistical validation parameters (SD = 0.081; R^2 = 0.903; Q^2 = 0.869; $r^2_{pred} = 0.861$; F = 247.2). This result suggests that the 3D-QSAR combinatorial model can be used to search for new 3VHE inhibitors and predict their potential activity. Based on the combinatorial pharmacophore model, a virtual screening of the Enamine database was performed. Compounds selected after virtual screening were subjected to molecular docking protocols (HTVS, SP, XP and IFD). Twenty new active compounds have been identified and their absorption, distribution, metabolism and excretion (ADME) property calculated using Schrödinger's Qikprop module. These results suggest that these new compounds could constitute new chemical starting points for further structural optimization of 3VHE inhibitors.

Keywords

Rhodanine, Pharmacophores, 3D-QSAR, Molecular Docking

1. Introduction

Prostate cancer accounts for 40% of all cancers affecting men. The incidence and mortality of prostate cancer continue to rise and is a major health problem in the world. It is the most common newly diagnosed cancer in men and has a very high death rate. This cancer death rate in men is second behind lung cancer [1]. Many factors of genetic, toxicological and diet-related origin seem to be involved in the development of this cancer. The treatment suggested to the patient depends on the size of the tumor in cancer. Doctors also take into account the evolutionary nature of it and the general state of health of the person. The treatment depends on the stage of advancement. The main treatment methods for prostate cancer are surgery, radiotherapy (external radiotherapy), active monitoring (which makes it possible to postpone the start of treatment), hormone therapy and chemotherapy. However, fundamental questions remain about the prevention and treatment of prostate cancer. Treatment for metastatic disease is strictly palliative and there is still no treatment for the disease. The thiazolidin-2,4-diones, rhodanine derivatives, five-membered heterocyclic compounds, have a wide range of biological activities that include antioxidants [2], anti-inflammatory [3] [4], antibacterial [5] [6], antifungals [7] [8], and the most important being the anticancer activity [9] [10] [11]. The presence of rhodanine in a very wide range of compounds possessing very varied biological properties makes it an important compound in the search for new drugs. Computer-aided design methods which include a series of techniques for discovering, designing and improving chemicals in silico are of considerable support in this research. [12] [13]. Five-membered heterocycles, which exhibit interesting biological activities as well as important industrial applications, are such potential targets [14]. This is the context in which our work, which aims to identify, using in silico methods, new prostate cancer inhibitors with rhodanine and its derivatives as base molecules.
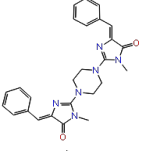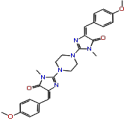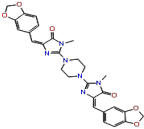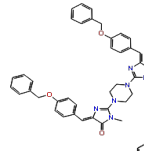
2. Materials and Methods
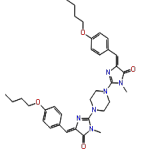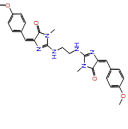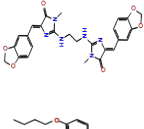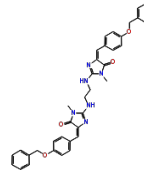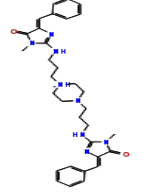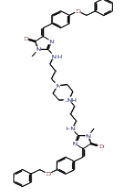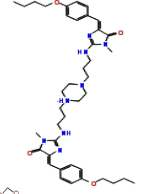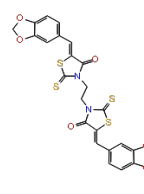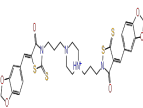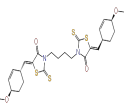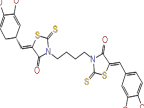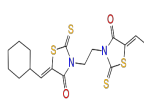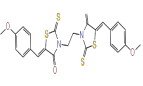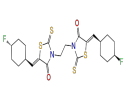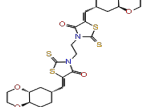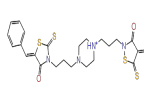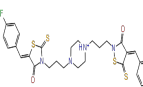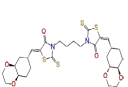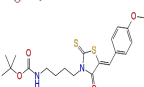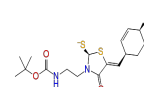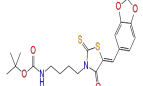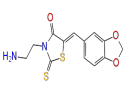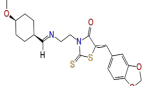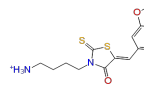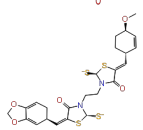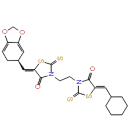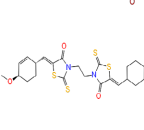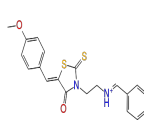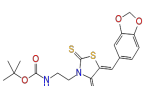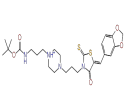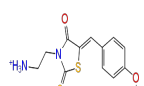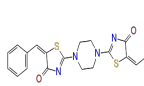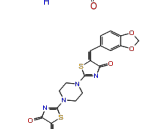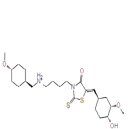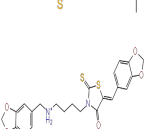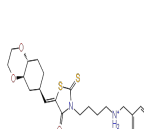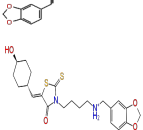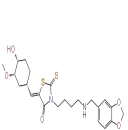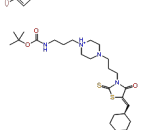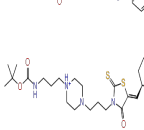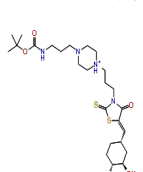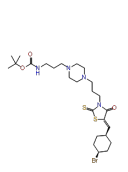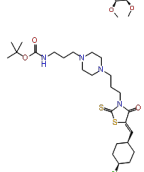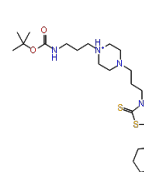
2.1. Selection of Biological Dataset

A data set of 74 rhodanine derivatives with their anticancer activity IC50 (μM) as inhibitors of prostate cancer (PC3) was extracted from the work of Coulibaly *et al.* [15]. All molecular structures and activity data used for pharmacophore modeling, 3D-QSAR study, virtual screening and molecular docking are shown in Table 1. For these studies, the inhibitory activities (IC50 values in M) for each compound were changed to a negative logarithm of IC_{50} (pIC_{50}). The pIC50 values were used as dependent variable for the development of the model in the 3D QSAR. All compounds have a similar structure and bioassay method.
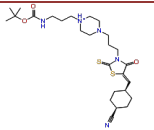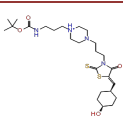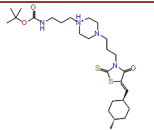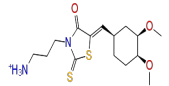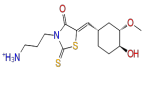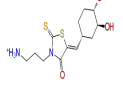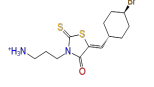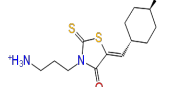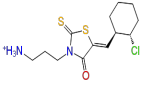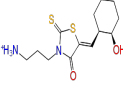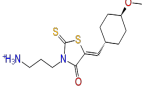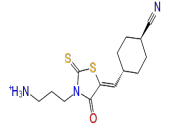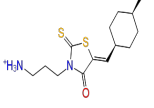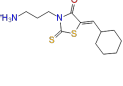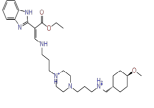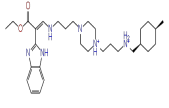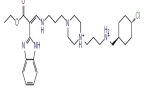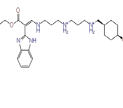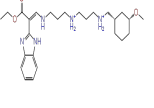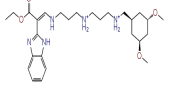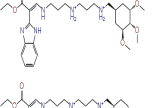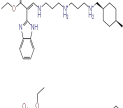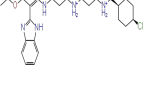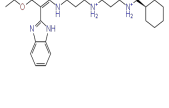
2.2. Ligand Preparation

The 3D structures of the ligands were generated using the construction panel in Maestro and optimized using the LigPrep module [16]. Partial atomic charges

Table 1. Structures and pIC50 of PC3 inhibitors.

Ligands	2D structure	Activity PC3	Ligands	2D structure	Activity PC3	Ligands	2D structure	Activity PC3	Ligands	2D structure	Activity PC3
F1		3.921	F2		3.947	F3		3.921	F4		3.987
F5		3.979	F6		4.125	F7		4.229	F8		4.041
F9		3.987	F10		4.252	F11		4.091	F12		4.041
F13		3.975	F14		3.914	F15		3.951	F16		3.987
F17		3.951	F18		3.9	F19		3.665	F20		3.955
F21		3.896	F22		3.917	F23		4.036	F24		3.959
F25		3.903	F26		4.027	F27		3.962	F28		3.943
F29		3.959	F30		3.924	F31		3.987	F32		3.991
F33		4.027	F34		4.268	F35		4.032	F36		4.187
F37		4.071	F38		4.387	F39		4.292	F40		4.409
F41		4.42	F42		4.215	F43		4.495	F44		4.31
F45		4.638	F46		4.538	F47		4.201	F48		4.481

Continued

F49	4.538	F50	4.569	F51	4.337	F52	4.174
F53	4.155	F54	4.000	F55	4.187	F56	4.114
F57	4.194	F58	4.268	FF59	4.18	F60	4.066
F61	4.114	F62	4.071	F63	4.921	F64	4.959
F65	4.886	F66	4.18	F67	4.143	F68	4.301
F69	4.086	F70	4.553	F71	4.42	F72	4.022
F73	4.143	F74	4.187				

were assigned and possible ionization states were generated at a pH of 7.0 ± 2.0. The OPLS_2005 force field was used for optimization of the production of the low energy ligand conformer [17]. Energy minimization was performed for each ligand until it reached a root mean square deviation threshold of 0.01 Å.

2.3. Pharmacophore Model Generation

Schrödinger's Phase module for ligand-based drug design was used to develop pharmacophore hypotheses [18]. Before generating the pharmacophoric model, Phase first recruits the Glide XP tool to anchor the ligand already bound to the active site of the protein under study and selects the best-ranked pose for the generation of the pharmacophores model. The chemical characteristics of all ligands were defined by six characteristics of pharmacophores: H-bond acceptor (A), H-bond donor (D), hydrophobic group (H), negatively charged group (N), positively charged group (P) and aromatic ring (R). An active analogue approach was used to identify common pharmacophore hypotheses, in which common pharmacophores were selected from the conformations of the active ligand set using a hierarchical partitioning technique that groups similar pharmacophores according to their inter-site distances [19]. The resulting pharmacophores were then noted and classified. Scoring was done to identify the best candidate hypothesis, which provided an overall ranking of all hypotheses. The scoring algorithm included contributions from site point and vector alignment, volume over-

lap, selectivity, number of paired ligands, relative conformational energy, and biological activity [19].

2.4. Pharmacophore Validation

The validation of a pharmacophore model is a fundamental first step that must be performed to prove its accuracy and specificity in the selection of active molecules, while guiding the virtual screening of ligands from a database. In the present study, a set of 324 decoy molecules extracted from Directory of Useful Decoys (http://dude.docking.org/) [20] [21] enriched with 9 active molecules was used. Before validation, the preprocessing of the active and decoy datasets was performed using the LigPrep module. All possible ionizable states as well as tautomeric forms at a pH range of 7.0 ± 2.0 were generated using LigPrep module [16]. For each compound, at most 32 conformers were generated by default and low energy stereoisomers with correct chirality were engaged for further analysis. The hypothesis validation tool of the Phase module [22] has been used. This tool uses the hypothesis file and the decoy and active dataset as input to calculate the performance parameters mentioned above. Various statistical parameters including Enrichment Factors (EF), Robust Initial Improvement (RIE), Boltzmann Enhanced Discrimination of Receiver Operating Characteristic (BEDROC), Area Under Accumulation Curve (AUC) and receiver operating characteristics (ROC) were calculated to validate the hypothesis [23].

2.5. Guner-Henry Score Validation

Güner-Henry scoring method is applied for quantification of model selectivity and evaluation of model effectiveness of similarity search. This scoring evokes the actives from a molecule dataset consisting of known active and inactive molecules. This scoring system ranges from 0 to 1, where 0 specifies a null model and 1 specifies an ideal model. The score is expected to be greater than 0.7 [24]. The formulas used for calculating *GH* score are given below:

$$GH = \left(\frac{H_a (3A + H_t)}{4H_t A} \right) \left(1 - \frac{H_t - H_a}{D - A} \right)$$

$$\%A = \frac{H_a}{A} \times 100; \ \%Y = \frac{H_a}{H_t} \times 100; \ EF = \frac{H_a / H_t}{A / D}$$

where H_a is the number of actives in the hits list (true positives), A is the number of active compounds in the database, H_t is the number of hits retrieved, D is the number of compounds in the database, $\%A$ is the percentage of known active compounds obtained from the database, $\%Y$ is the percentage of known actives in the hits list, EF is the enrichment of the concentration of actives by the model relative to random screening without a pharmacophoric approach. Güner-Henry score is considered as a relevant metric, it takes into account both percent yield of actives in a database ($\%Y$) and the percent ratio of actives in the hit list ($\%A$).

2.6. 3D-QSAR

QSAR modeling was carried out by dividing the data set (74 molecules) into a training set (75%) and a test set (25%) randomly. PHASE presents two options for the alignment of the 3D structure of molecules: the pharmacophore-based alignment and the atom-based alignment [19] [25]. In this study, we used an atom-based QSAR model, which is more useful in explaining the structure-activity relationship. In atom-based QSAR, a molecule is treated as a set of overlapping van der Waal spheres. Each atom (and therefore each sphere) is classified into one of six categories according to a set of simple rules: hydrogens attached to polar atoms are classified as donors of hydrogen bonds (D); C-H carbons, halogens and hydrogen are classified as hydrophobic/nonpolar (H); atoms with an explicit negative ionic charge are classified as negative ionic (N); atoms with an explicit positive ionic charge are classified as positive ionic (P); nonionic nitrogen and oxygen are classified as electron attractors (W); and all other types of atoms are classified as miscellaneous (X).

For the purposes of QSAR development, the van der Waal models of the aligned molecules of training set were placed in a regular grid of cubes, each cube being assigned zero or more "bits" to account for the different types of atoms in learning set that occupy the cube. This representation results in binary-valued occupancy models that can be used as independent variables to create partial least squares (PLS) QSAR models. A five-component model (PLS factor) with good statistics was obtained for the dataset. The statistical quality of the generated QSAR models was judged by parameters such as the regression coefficient (R^2), cross validation (Q_{CV}^2), the variance (F), the confidence interval (P), the mean squared error (RMSE) and Pearson's coefficient r [26].

2.7. High Throughput Virtual Screening and Molecular Docking

The molecules obtained after pharmacophore screening were filtered by High Throughput Virtual Screening (HTVS), followed by Glide docking SP (standard precision) and XP (extra precision) at the crystal structure binding sites with Glide. The co-crystallized ligand has been centralized for grid generation using the grid generation tools in Glide. MM-GBSA post-docking minimization (Molecular Mechanical Energies Combined with Generalized Born and Surface) was performed to optimize the geometries of the molecules recovered, and the 10% of the molecules recovered from each step were selected for the next level. Finally, all non-peptide molecules (peptide compounds are orally degradable) were run on the Glide XP molecular docking system, using the 3VHE crystal structure to estimate the docking scores of the resulting molecules after screening.

2.8. Induced Fit Docking

A molecular docking method, known as induced fit docking (IFD) [27], where the receptor is flexible in the docking study, has been performed. The energy minimisation of the protein structure was performed using the OPLS_2005 force

field. The prepared molecules were docked to the rigid protein using Glide with the default parameters. Energy minimisation was applied on the crystal structure of PDB code: 3VHE. XP molecular docking was used for initial docking and 21 ligand poses were maintained for protein structure refinement. Schrödinger's 2017-4 Prime module, was used to refine residues within 5.0 Å of the ligand poses and induced fit protein-ligand complexes were developed. After these refinements [28], the ranking of each of the 21 complexes was performed by Prime energy. Complex structures with an energy less than 30 kcal·mol^{-1} were re-docked for the final step of scoring. Each ligand was docked into each refined low energy receptor structure developed in the refinement step. The binding affinity of each complex was estimated by the docking score. The lowest negative docking score and IFD score was considered as a more favourable binding condition with the active site of 3VHE.

2.9. ADME Prediction

QikProp tool of Schrodinger [29] was applied to predict the druggable property of ten best hits by assessing the ADME profile. During this, the Lipinski rule of five and various descriptors like QPlogHERG, QPPCaco, QPlogBB, and % human oral absorption were calculated.

3. Results and Discussion

3.1. Generation of Pharmacophoric Models

For the modeling of pharmacophores, a set of 74 molecules in the activity range on the logarithmic scale (3.665 - 4.959) were selected. Compounds with a pIC50 activity > 4.4814 were selected as active while those with pIC50 < 4.0409 were considered inactive. The selected active and inactive molecules were used to test the specificity of the pharmacophore hypothesis and to define the excluded volumes. Models of pharmacophores containing 5 sites were generated using three features: hydrogen bond acceptor (A), hydrophobic (H) and aromatic ring (R). The survival score parameter gives a general ranking to all the pharmacophoric models generated and was used as selection criteria for the pharmacophores models. The best pharmacophores models obtained based on the site score, vector score and volume score parameters which lead to the survival score and BEDROC score parameters have been reported in Table 2. A good pharmacophores model is characterized by a high value of the parameters. Survival score. The survival score value of all pharmacophoric models generated varies between 4.911 and 5.129. Model AAHHR-3 had the highest value while model AAAHR-8 gave the lowest value for survival score.

3.2. Analysis of Pharmacophoric Models

The pharmacophoric models constructed were validated using a set of parameters (Table 3) in a database containing 324 decoy molecules, collected using 9 inhibitors of prostate cancer cells (PC3) which were not used in the construction

Table 2. Pharmacophores model and scoring parameters.

Pharmacophore models	Survival Score	Site Score	Vector Score	Volume Score	Selectivity Score	Inactive Score	Adjusted Score	BEDROC Score	Phase Hypo Score
AAAHR_3	5.129	0.834	0.947	0.565	1.606	1.189	3.940	0.721	1.029
AAAHR_1	5.201	0.866	0.944	0.609	1.606	1.227	3.974	0.715	1.027
AAAHR_2	5.169	0.868	0.934	0.599	1.592	1.229	3.940	0.703	1.013
AAAHR_4	5.099	0.849	0.945	0.538	1.592	1.152	3.948	0.702	1.008
AAHHR_3	5.165	0.742	0.924	0.560	1.825	1.459	3.706	0.639	0.949
AAHHR_1	5.273	0.782	0.933	0.623	1.821	1.415	3.858	0.630	0.946
AAHHR_2	5.244	0.782	0.906	0.625	1.818	1.444	3.801	0.631	0.946
AAHHR_4	5.126	0.632	0.934	0.617	1.830	1.714	3.412	0.638	0.945
AAHHR_5	5.125	0.641	0.942	0.595	1.833	1.719	3.406	0.623	0.931
AAAHR_6	4.914	0.642	0.910	0.621	1.627	1.587	3.327	0.632	0.927
AAAHR_5	4.957	0.709	0.910	0.595	1.598	1.694	3.263	0.626	0.924
AAAHR_7	4.911	0.710	0.910	0.569	1.608	1.711	3.200	0.626	0.920
AAAHR_8	4.911	0.651	0.911	0.572	1.600	1.660	3.250	0.624	0.919

Table 3. Characteristics of the best pharmacophores models obtained after validation.

N.°	HYPOTHESES	D	A	H_t	H_a	%Y	%A	FP	FN	EF	ROC	RIE	BEDROC	AUC	GH
1	AAHHR_5	333	9	10	9	90.00	100	1	0	33.30	0.99	14.6	0.99	0.98	0.92
2	AAHHR_4	333	9	12	9	75.00	100	3	0	27.75	0.99	14.01	0.95	0.98	0.80
3	AAHHR_3	333	9	16	9	56.25	100	7	0	20.81	0.98	12.14	0.80	0.97	0.66
4	AAHHR_1	333	9	14	9	64.29	100	5	0	23.79	0.98	13.37	0.89	0.97	0.72
5	AAAHR_8	333	9	10	9	90.00	100	1	0	33.30	1	14.69	0.99	0.98	0.92
6	AAAHR_7	333	9	13	9	69.23	100	4	0	25.62	0.99	13.08	0.82	0.97	0.76
7	AAAHR_6	333	9	14	9	64.29	100	5	0	23.79	0.98	12.04	0.34	0.97	0.72
8	AAAHR_5	333	9	16	9	56.25	100	7	0	20.81	0.98	11.68	0.83	0.96	0.66

of pharmacophoric models. The pharmacophore obtained were used for the screening of the database using the phase software screening tool implemented in the Schrödinger suite version 17-4. The ability of a pharmacophore to differentiate between active agents and decoys is given by the enrichment factor EF. The EF scores (1%) of the models obtained are in the range 20.81 - 33.30, indicating that these models are all able to identify assets from a large dataset of compounds [30].

The position of the actives in relation to the compounds classified in an ordered manner corresponds to the ROC value. This value varied between 0 and 1 where a value greater than or equal to 0.7 is considered an appropriate performance measurement value [31]. In the present study, ROC value of between 0.98

and 1 indicates that the pharmacophores models obtained have a strong capacity for selecting active molecules. In addition, the % screen graph and the ROC graph (Figure 1) revealed the sensitivity and specificity of recognizing active molecules. BEDROC measurements measure early recognition of database assets and range from 0 to 1 [32]. We considered $\alpha = 20.0$ for the BEDROC metric, which means that 80% of BEDROC results come from the first 8% of the molecules classified [31]. Therefore, a substantial BEDROC value ($\alpha = 20.0$) between 0.80 and 0.99 suggested the early detection of active compounds in the database. The selection of the best hypotheses was carried out using the Güner-Henry (GH) scoring method. The analysis of GH notation was carried out by calculating the following variables: %A is the percentage of known active compounds extracted from the database (precision), H_a is the number of assets in the list of results (true positives), A is the number of active compounds in the database, %Y, the percentage of known assets in the results list, H_t is the number of results retrieved, D is the number of compounds in the database, EF is the enrichment of the active concentration by the model compared to the random screening without any pharmacophore approach and GH is the Güner-Henry score. Models 1 and 5 succeeded in recovering 90% of the active compounds and a GH score of 0.92 indicated the good quality of these models (Table 3). All these enrichment results suggest that the pharmacophores models generated are satisfactory for the recovery of the assets of a large database of molecules.

Based on the GH parameter, the models with the greatest power of selectivity for active molecules are AAHHR_5 and AAAHR_8 (GH = 0.922). The AAHHR_5 hypothesis is characterized by two attractor sites (A), two hydrophobic sites (H) and one aromatic site (R). The other model, AAAHR_8 is represented by three attractor sites (A), a hydrophobic site (H) and an aromatic site (R). The distances and angles between the different sites of the models are given in Table 4 and Table 5, respectively and illustrated in Figure 2. Interactions less than 3.1 Å are considered to be strong. Those between 3.1 Å and 3.55 Å are assumed to be average while those greater than 3.55 Å are low [33].
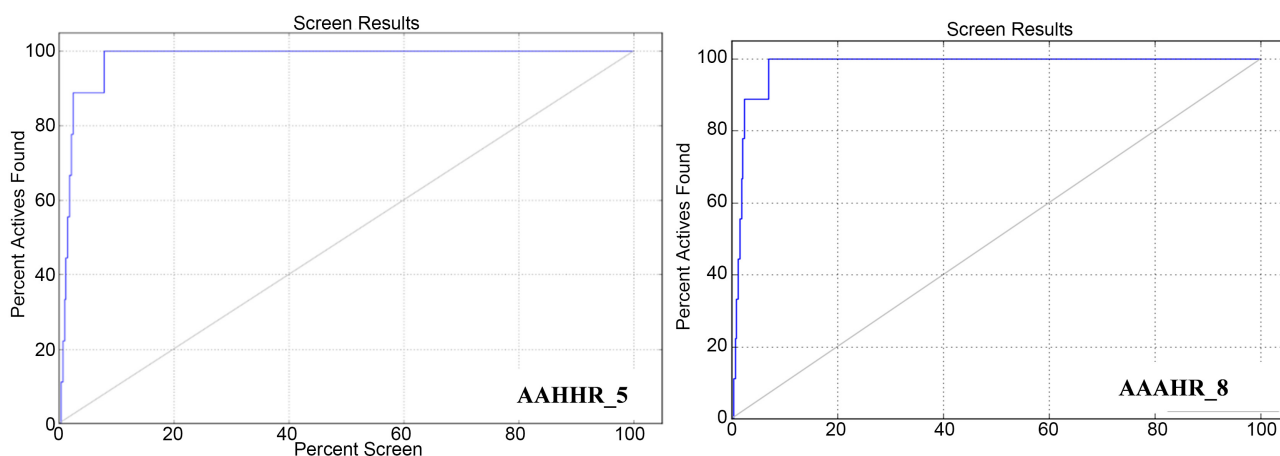
Figure 1. Roc curve of the pharmacophores models AAHHR_5 and AAAHR_8.
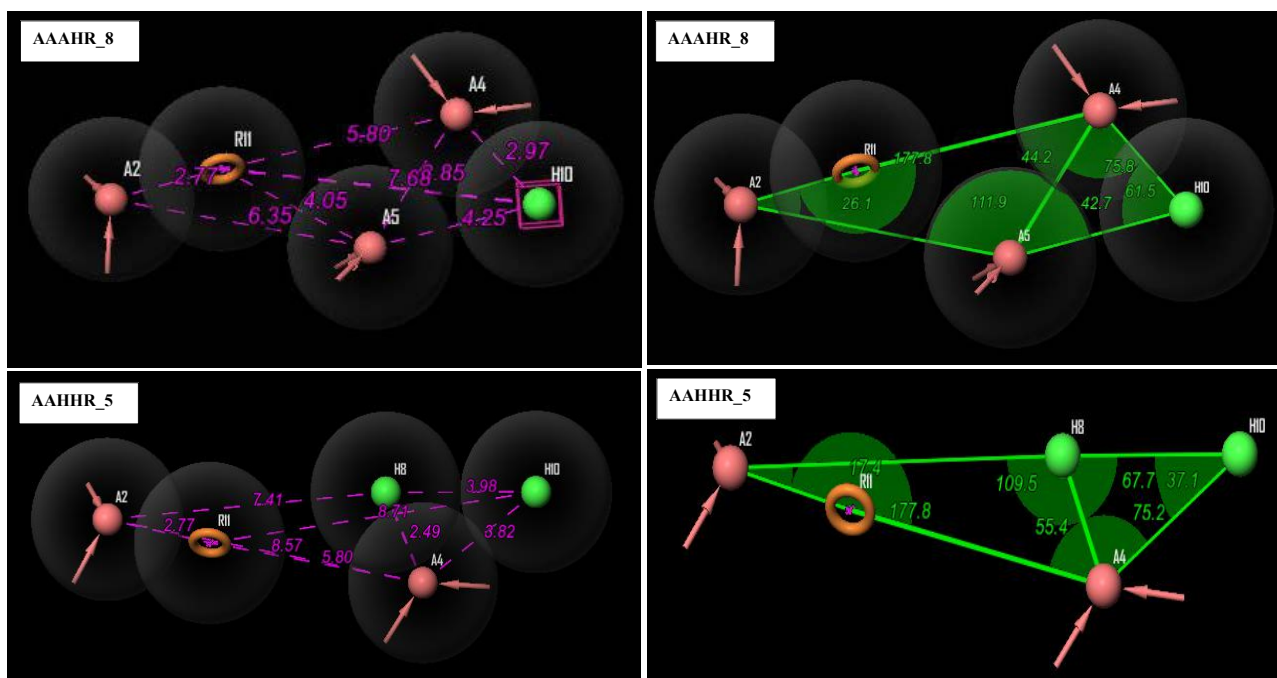
Figure 2. Distances and angles between pharmacophoric sites of models AAHHR_5 and AAAHR_8.

Table 4. Distance between the different pharmacophoric sites of models AAHHR_5 and AAAHR_8.

Site 1	Site 2	range (Å)	Site 1	Site 2	range (Å)
model AAHHR_5					
A2	**R11**	**2.17**	R11	H8	4.84
A2	A4	8.57	R11	H10	8.71
A2	H8	7.41	**A4**	**H8**	**2.49**
A2	H10	11.32	A4	H10	3.82
R11	A4	5.80	H8	H10	3.98
model AAAHR_8					
A2	**R11**	**2.77**	A4	R11	5.80
A2	A5	6.35	A5	A4	3.85
A2	H10	10.30	A5	H10	4.25
A2	A4	8.57	**A4**	**H10**	**2.97**
R11	A5	4.05	R11	H10	7.68

Table 5. Angles between the different pharmacophoric sites of the AAHHR_5 and AAAHR_8 models.

Site 1	Site 2	Site 3	Angle (°)	Site 1	Site 2	Site 3	Angle (°)
model AAHHR_5							
H10	H8	A4	67.7	H8	R11	A2	152.8

Continued

H10	H8	R11	161.3	H8	A2	R11	17.4
H10	H8	A2	166.3	A2	H8	R11	9.8
H10	A4	H8	75.2	H8	R11	A4	25.0
H10	R11	H8	8.4	H8	A4	R11	55.5
H10	A2	H8	4.8	A4	H8	R11	99.6
H8	H10	A4	37.1	A4	A2	R11	1.5
R11	H10	H8	10.3	A2	A4	R11	0.7
A4	H10	A2	36.6	A4	H10	R11	31.3
A4	R11	H10	20.0	R11	A4	H10	128.7

model AAAHR_8

Site 1	Site 2	Site 3	Angle (°)	Site 1	Site 2	Site 3	Angle (°)
H10	A4	A5	75.8	A2	R11	A5	136.3
H10	A5	A4	42.7	A2	R11	A4	177.8
H10	A4	R11	118.6	A2	R11	H10	158.0
H10	A4	A2	117.9	A2	A4	A5	43.4
H10	A5	R11	135.3	A4	A2	A5	24.6
H10	R11	A5	22.9	A5	R11	A2	136.3
H10	R11	A2	158.0	A5	A2	R11	26.1
H10	R11	A4	19.8	A2	A5	R11	17.5
H10	A2	A5	11.1	A5	H10	A4	61.5
A2	A5	R11	17.5	A4	A5	R11	94.4
A4	R11	A5	41.4	A5	A4	R11	44.2

3.3. Development and Validation of 3D-QSAR Models

Using the phase software of Schrödinger suite, we generated a set of 3D-QSAR models using the "atom-based QSAR" module which gradually incorporates PLS (Partial Least Square) regression factors. To build the model the grid spacing parameter was set to 1 Å, the PLS factors were set to 5 and the variables with |t-values| < 2.00 have been eliminated. A 3D-QSAR model was generated with 74 ligands which were randomly divided into the test set (56 ligands) and validation set (18 ligands). The Phase module generated a total of 5 models with the different statistical parameters which are presented in Table 6. The model with a PLS factor equal to 2 was considered for further analysis because a small difference between biological activity and biological activity was obtained. Predicted activity with a standard deviation of 0.10005 (Table 6). The curve validating the accuracy of the 3D-QSAR model is presented in Figure 3 which illustrates the evolution of the predicted biological activity of the molecules as a function of their experimental biological activities. We observe a good linear correlation between the activities predicted by the model and the experimental activities.

Table 6. Experimental and predicted values of the molecules of the test set (training set) and the validation set (test set) based on the PLS factor 2.

ligands Code	QSAR set	Activity	Pred activity	residual
F45	training	4.638	4.529	−0.110
F46	training	4.538	4.420	−0.117
F47	training	4.201	4.420	0.220
F49	training	4.538	4.481	−0.056
F50	training	4.569	4.478	−0.090
F57	training	4.194	4.152	−0.042
F58	training	4.268	4.164	−0.104
F59	training	4.180	4.154	−0.027
F60	training	4.066	4.148	0.083
F61	training	4.114	4.163	0.050
F62	training	4.071	4.156	0.085
F63	training	4.921	4.952	0.031
F64	training	4.959	4.962	0.003
F66	training	4.180	4.283	0.103
F67	training	4.143	4.231	0.089
F68	training	4.301	4.362	0.061
F69	training	4.086	4.138	0.052
F70	training	4.553	4.296	−0.256
F72	training	4.022	4.257	0.235
F74	training	4.187	4.157	−0.030
F1	training	3.921	4.031	0.110
F2	training	3.947	3.931	−0.016
F3	training	3.921	3.940	0.019
F4	training	3.987	3.994	0.007
F5	training	3.979	3.977	−0.002
F6	training	4.125	4.181	0.056
F7	training	4.229	4.150	−0.079
F8	training	4.041	4.041	0.000
F9	training	3.987	3.995	0.008
F10	training	4.252	4.203	−0.049
F11	training	4.091	4.085	−0.006
F13	training	3.975	3.900	−0.075
F14	training	3.914	4.008	0.094
F15	training	3.951	3.947	−0.004
F16	training	3.987	4.005	0.018
F17	training	3.951	3.974	0.023

Continued

F18	training	3.900	3.965	0.065
F19	training	3.665	3.571	−0.094
F21	training	3.896	3.888	−0.008
F22	training	3.917	3.924	0.007
F23	training	4.036	3.957	−0.080
F24	training	3.959	3.973	0.015
F25	training	3.903	3.998	0.095
F27	training	3.962	3.951	−0.011
F29	training	3.959	3.941	−0.018
F30	training	3.924	3.930	0.006
F31	training	3.987	3.899	−0.088
F32	training	3.991	4.025	0.033
F33	training	4.027	4.014	−0.013
F34	training	4.268	4.220	−0.047
F35	training	4.032	4.039	0.007
F36	training	4.187	4.183	−0.004
F38	training	4.387	4.354	−0.033
F39	training	4.292	4.280	−0.012
F40	training	4.409	4.356	−0.052
F41	training	4.420	4.370	−0.050
F43	test	4.495	4.376	−0.119
F44	test	4.310	4.420	0.110
F48	test	4.481	4.403	−0.078
F51	test	4.337	4.422	0.085
F52	test	4.174	4.186	0.012
F53	test	4.155	4.103	−0.052
F54	test	4.000	4.134	0.134
F55	test	4.187	4.157	−0.030
F56	test	4.114	4.155	0.042
F65	test	4.886	4.840	−0.046
F71	test	4.420	4.249	−0.171
F73	test	4.143	4.194	0.051
F12	test	4.041	4.080	0.039
F20	test	3.955	3.906	−0.049
F26	test	4.027	4.028	0.002
F28	test	3.943	4.035	0.092
F37	test	4.071	3.946	−0.125
F42	test	4.215	4.195	−0.020
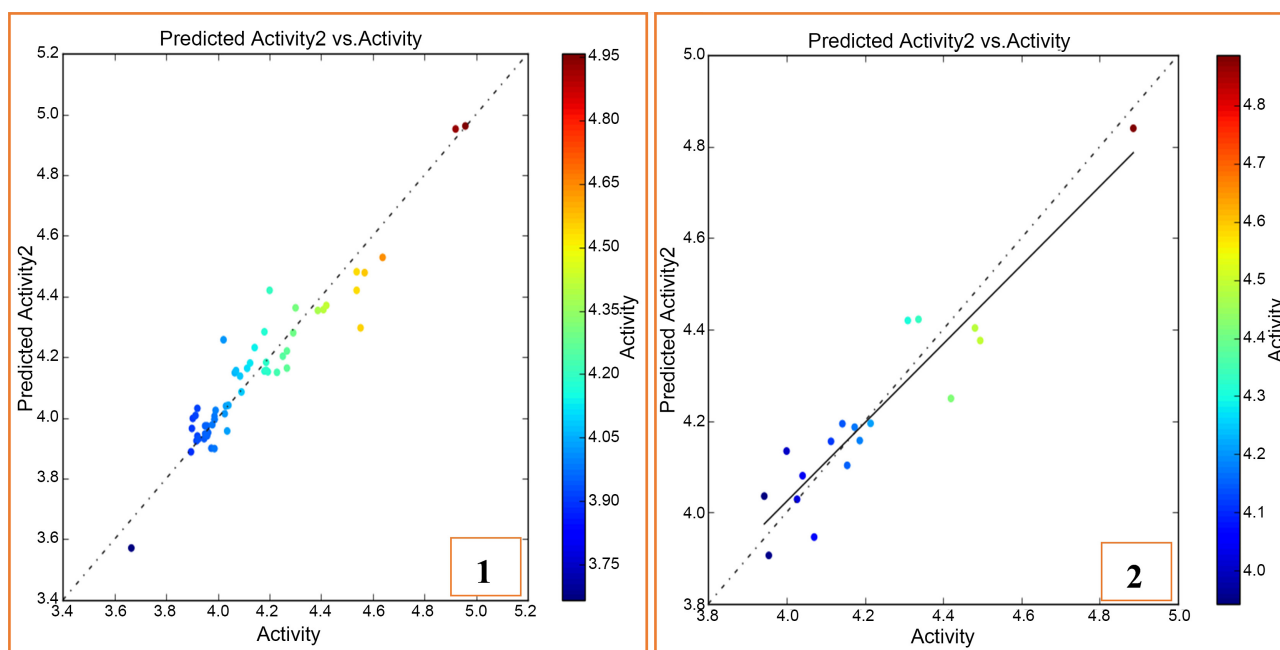
Figure 3. Line scatter plot illustrating the correlation of actual activity versus predicted activity for the test (1) and validation (2) set using an atom-based 3D-QSAR model.

The residual scale which is the difference between the experimental activity and the predicted activity was used to rank the predictions. Residues less than 0.8 were considered good predictions while residues between 0.8 and 1.6 were considered weak predictions. Residues greater than 1.6 were considered bad predictions [34]. The results obtained show that all the molecules have good predictions as a function of their residual scale (Table 6).

To provide reliable predictability, a good model must undergo internal and external validation. The predictive power of the generated 3D-QSAR model was analysed using a set of 18 compounds and the statistical significance of the model was obtained using a PLS factor 2. The robustness of the model to predict active molecules was considered as a function of various internal and PLS parameters, including cross-validation coefficient (Q^2), the correlation coefficient between predicted and experimental biological activity (R^2), the standard deviation (SD), the mean squared error (RMSE), the variance (F), the significance level of variance ratio (P), Pearson's correlation coefficient (Pearson-r) and model stability (Table 7). For the PLS factor 2, the regression coefficient ($R^2 = 0.9032$) on the one hand and cross-validation coefficient ($Q^2 = 0.9077$) on the other hand, indicate that the model has good internal predictive power. In addition, the very large value of the variance ($F = 247.2$) with a small value of $P = 1.348\text{e}{-}27$, low SD (0.0813), low RMSE (0.08) and high value of Pearson-r 0.9330 confirmed the importance of the selected model (Table 7). There is little difference between predicted and biological activities of the test and validation sets. This small difference highlights the effectiveness of 3D-QSAR model. The value $R^2 - Q^2 = 0.0336 < 0.3$, all internal statistical parameters are well within the defined range,

Table 7. Result of the quantitative structure-activity relationship (QSAR) of the developed model.

Factor	SD	R^2	R^2_{CV}	$R^2_{Scramble}$	Stability	F	P	RMSE	Q^2	$R^2 - Q^2$	Pearson-r
1	0.1090	0.8227	0.3919	0.5179	0.661	250.6	6.12e−22	0.10	0.8203	0.0024	0.9287
2	0.0813	0.9032	0.4311	0.7654	0.58	247.2	1.34e−27	0.08	0.8695	0.0336	0.9330
3	0.0697	0.9303	0.4271	0.8462	0.535	231.2	4.82e−30	0.09	0.8567	0.036	0.9272
4	0.0633	0.9435	0.4103	0.8817	0.516	212.9	3.79e−31	0.09	0.8389	0.1046	0.9177
5	0.0592	0.9516	0.3992	0.9036	0.495	196.6	1.25e−31	0.10	0.8291	0.1225	0.9116

SD. regression standard deviation; R^2 is for the regression coefficient; F is the ratio of the model variance to the observed activity variance (variance ratio); P: significance level of the variance ratio; RMSE: mean square error. Q^2 directly analogous to R^2 but based on the predictions of the test set is a validation metric calculated using observations (y-axis) and predictions (x-axis) and the Pearson-r value for the correlation between predicted and observed activity for the test set; RMSE RMS error in test set predictions.

but external statistical validation is also essential for greater reliability of the selected model.

The atomic contributions of the molecules were analysed in order to understand 3D-QSAR model obtained and to clarify the design requirements for developing more potent human liver cancer inhibitors. The result is shown in **Table 8**. According to the results of the constructed QSAR model, the hydrophobic contributions/nonpolar substituents. Electron-withdrawing groups favorably contribute to the biological activity of the compounds studied.

3.4. Analysis of External Statistical Validation

In order to assess the external predictive capacity of 3D-QSAR model obtained. The Golbraikh-Tropsha parameters and Roy's metric were used to calculate the external predictive correlation coefficients r^2_{pred}, CCC, $Q^2_{F_1}$ and $Q^2_{F_2}$ [35]. In **Table 9**, the values of r^2_{pred} of 3D-QSAR models and high values of CCC, $Q^2_{F_1}$ and $Q^2_{F_2}$ shows the robustness and efficiency of the external prediction capability of 3D-QSAR model. This external prediction capability indicates the reliability of 3D-QSAR model in predicting the biological activity of new compounds. As can be seen in **Table 8**, the established models also meet the criteria of Golbraikh-Tropsha and Roy. According to the data in **Table 10**, these criteria are present in the established 3D-QSAR model. Also the result showed that the established 3D-QSAR model was free from systematic error and can therefore be applied to the prediction of the biological activity of the ligands of the test set.

Table 9 shows the performance parameters based on the MAE criteria [36] for the external validation tests of the 3D-QSAR model. If a QSAR model follows the criteria: MAE ≤ 0.1 × range of the test set and MAE ± 3σ ≤ 0.2 × range of the test set then the model can be considered a good predictor. According to the data in **Table 9**, these criteria are present in the established 3D-QSAR model. Also the result showed that the established 3D-QSAR model was free from systematic error and can therefore be applied to the prediction of the biological activity of ligands of the validation set.

Table 8. Contribution of the atom-type fraction.

Factors	H-bond donor	Hydrophobic/ non-polar	Negative ionic	Positive ionic	Electron-withdrawing	Other
1	0.051	0.573	0.005	0.050	0.190	0.132
2	0.058	0.574	0.005	0.054	0.188	0.122
3	0.063	0.571	0.004	0.058	0.190	0.115
4	0.064	0.561	0.003	0.057	0.194	0.121
5	0.065	0.556	0.002	0.057	0.196	0.123

Table 9. Statistical properties calculated for the external validation of the developed QSAR models.

Parameters of GOLBRAIK-TROPSHA	
r^2_{pred}	0.86107
R^2	0.8704
R^2_0	0.8703
R'^2_0	0.8485
$\dfrac{R^2 - R^2_0}{R^2}$	0.0001148
$\left| R^2_0 - R'^2_0 \right|$	0.0218
k	1.00167
k'	0.99794
ROY parameters	
$\overline{r^2_m}$	0.8245
$\overline{\Delta r^2_m}$	0.0722
$Q^2_{F_1}$	0.8694
$Q^2_{F_2}$	0.8694
CCC	0.9295

Table 10. Results of external statistical validation of the 3D-QSAR model by the MAE method.

Validation Parameters	parameters	PLS-2
Model biasness test	Systematic Error Result	Absent
Error-based metrics (for 100% data)	RMSEP (100% data)	0.0835
	SD (100% data)	0.0471
	SE (100% data)	0.0111
	MAE (100% data)	0.0698
Error-based metric (after removing 5% data with high residuals)	RMSEP (95% data)	0.0752
	SD (95% data)	0.0410
	SE (95% data)	0.0099
	MAE (95% data)	**0.0639**
	MAE + 3 * SD (95% data)	**0.1868**
RESULT (MAE-based criteria applied on 95% data)	**Prediction Quality**	**GOOD**

3.5. 3D-QSAR Visualization Map Analysis

Color maps provide information on positions which require a particular physicochemical property to enhance the cytotoxic activity of a ligand. The QSAR model displays the 3D features as cubes. The blue cubes show positive coefficients which are favorable while the red cubes show negative coefficients which are unfavorable characteristics for the activity. These maps give a clue of which functional group is desirable or undesirable at certain positions in a ligand. Their positive contribution is represented by blue cubes and their negative contribution is represented by red cubes. The compounds F64, F38 and F19 were selected as model molecules for the study of the resulting 3D QSAR model.

❖ Hydrogen Bond Donor interaction

For more active compound F64, the red region is around the oxygen atoms and also around the carbon between two nitrogen atoms of benzimidazole. Cyclohexane and the sulfur atoms of rhodanine are the areas of compound F38 around which the red cubes are concentrated. This indicates that substitutions at these positions by groups with more hydrogen bond donor property do not promote the inhibitory activity of the ligand in the active site of the 3VHE receptor. The blues regions are seen around the nitrogen atoms of the F64 ligand. For compound F38, the blue area is concentrated around the oxygen atoms and also around the carbon-carbon double bond close to rhodanine. Concerning the F19 molecule, the blue region is located around the two carbon atoms (C27, C30) located between the two rhodanine rings. These areas indicate that substitution at these positions with groups with greater hydrogen bond donor properties promotes the inhibitory activity of the ligand in the active site of the 3VHE receptor (Figure 4).

❖ Hydrophobic interactions

For more active compound F64, the red region is around the carbonyl group. For compound F38, the red cubes are located around the C2 and C4 carbon atoms of cyclohexane. Concerning compound F19, the red zone is located around the C30 carbon between the two rhodanine rings and also around the C=S double bond of rhodanine. Substitution by groups having more hydrophobic properties at these positions therefore it does not promote the inhibitory activity of the ligand in the active site of the 3VHE receptor. The blue regions of the most active compound F64 are observed around the cyclohexane and the piperazine ring including all the atoms located between these two rings. For compound F38, the blue region is observed around the sulfur atoms of rhodanine and also around the oxygen atoms bound to cyclohexane. For the F19 molecule, the blue cubes are located around two C=O double bonds and also the two nitrogen atoms of the rhodanine sites. These areas indicate that substitution at these positions by groups with strong hydrophobic properties promotes the inhibitory activity of the ligand in the active site of the 3VHE receptor (Figure 5).

❖ Electro-attractor interaction

Visual analysis of compound F64 indicates the presence of blue cubes at the
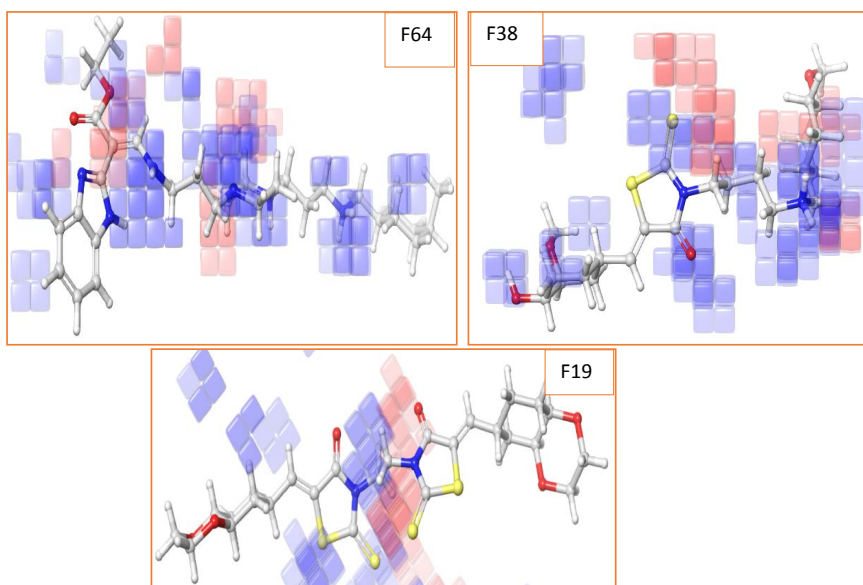
Figure 4. Overview of contour maps for 3D-QSAR hydrogen bond donor models for F64, F38 and F19.
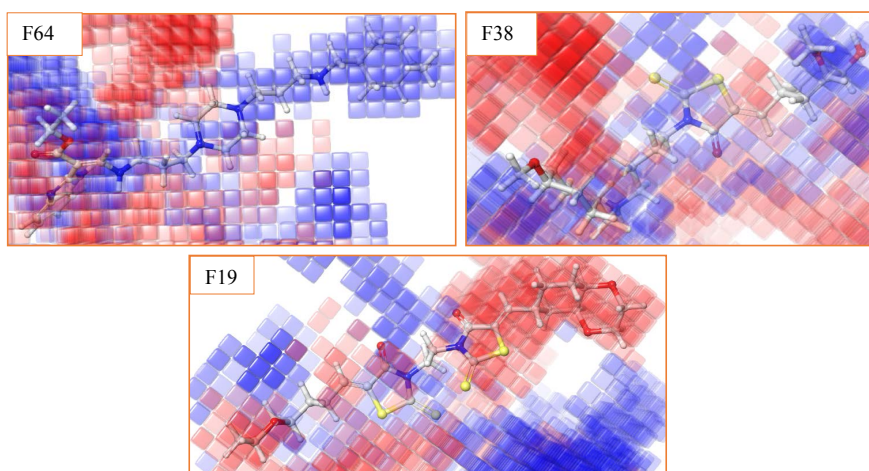
Figure 5. Overview of contour maps for 3D-QSAR models of hydrophobic interactions for F64, F38 and F19.

benzimidazole and two nitrogen atoms of the piperazine ring. For the F38 molecule, these blue cubes are seen around the oxygen and sulfur atoms. Regarding F19, the blue zone is observed around the carbon-carbon double bond linked to rhodanine. These blue regions indicate that substitution by compounds with more electron-withdrawing properties at these positions promotes the inhibitory activity of the ligand against the 3VHE receptor. The areas represented by the red cubes indicate that substitution with compounds with greater electron-withdrawing properties does not promote the inhibitory activity of the ligand in the active site of 3VHE receptor. For the F64 compounds this zone is located around the carbon atoms of the piperazine ring and the oxygen atoms. For compound F38, it is localized around the two cyclohexane rings and around

rhodanine. Regarding F19, we observe the red cubes around all the oxygen atoms of the molecule but also around the C=O double bonds of rhodanines (Figure 6).

3.6. Virtual Screening of the Enamine Chemical Library

The increasing numbers of genomic targets of therapeutic interest [37] and macromolecules (proteins, nucleic acids) for which a three-dimensional (3D) structure is available [36] make virtual screening techniques increasingly attractive for bioactive molecule identification projects [38]. Virtual screening is any computer search process in molecular databases that allows the selection of molecules. In this work, docking studies were performed using the Schrödinger Suite Glide grid-based method [39]. Virtual stepwise screening was performed using the Glide HTVS, SP and XP docking methodologies described above. All docking poses were scored with the MM-GBSA approach, as implemented in the Prime program of the Schrödinger software suite. After the Prime MM-GBSA analysis we retained the molecules with energies below −50 kcal/mol. To take into account the flexibility of the protein, the resulting set of molecules was subjected to the IFD protocol. The sequential virtual screening including the HTVS, SP, XP prime MM-GBSA and IFD protocols allowed us to select a total of 20 new molecules. Table 11 and Table 12 present some parameters of these obtained compounds as well as their 3D structures.

All the molecules obtained have a fitness score greater than 1.5, which means that they are well aligned with the pharmacophore hypotheses that enabled them to be found. The higher the fitness score, the better the structural alignment. The fitness scores of the leads are between 1.507 and 1.775. The compound PV-002558797812 found by the AAAHR_6 pharmacophore model with a fitness score of 1.772 is the highest ranked. The compound Z1694049401 found by the AAAHR_5 model with a fitness score of 1.716 follows. The compound Z1684534882 found by the pharmacophore model AAAHR_7 has the lowest fitness score with 1.507.
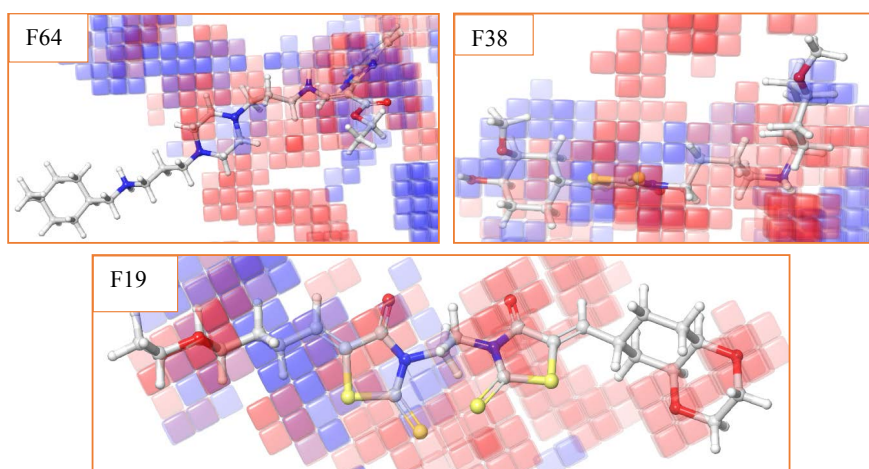
Figure 6. Overview of contour maps for 3D-QSAR models of electron-withdrawing interactions for F64, F38 and F19.

Table 11. Molecules retained after virtual screening by pharmacophore models and by molecular docking.

Code of the selected molecules	Align Score	Fitness	Phase Screen Score	Hypo ID	Matched Ligand Sites	Vector Score	Volume Score
Z1694049401	0.861	1.716	1.716	AAAHR_5	A(4) A(2) A(3) H(9) R(12)	0.920	0.514
Z2150792351	0.794	1.594	1.594	AAHHR_4	A(5) A(4) H(9) H(8) R(11)	0.934	0.321
PV-002427431755	0.735	1.641	1.641	AAAHR_6	A(4) A(2) A(5) H(9) R(12)	0.893	0.361
PV-002201035475	0.893	1.614	1.614	AAAHR_5	A(1) A(4) A(5) H(10) R(12)	0.829	0.529
PV-002215946839	0.753	1.701	1.701	AAAHR_8	A(2) A(3) A(4) H(8) R(11)	0.895	0.434
PV-002569833477	0.712	1.610	1.610	AAAHR_5	A(2) A(3) A(4) H(10) R(12)	0.792	0.411
PV-002109864487	0.881	1.584	1.584	AAHHR_4	A(4) A(3) H(8) H(9) R(11)	0.894	0.425
PV-001946374534	0.585	1.716	1.716	AAHHR_3	A(3) A(2) H(9) H(7) R(13)	0.873	0.331
PV-002273233325	0.703	1.587	1.587	AAAHR_8	A(2) A(3) A(4) H(9) R(11)	0.832	0.340
Z1683053210	0.681	1.582	1.582	AAAHR_6	A(4) A(6) A(1) H(9) R(14)	0.785	0.365
Z2121011596	0.878	1.560	1.560	AAHHR_4	A(1) A(3) H(9) H(7) R(11)	0.567	0.725
PV-002089512142	0.673	1.596	1.596	AAAHR_6	A(5) A(4) A(3) H(10) R(12)	0.349	0.808
PV-002342843731	0.559	1.528	1.528	AAAHR_6	A(2) A(3) A(4) H(10) R(14)	0.275	0.718
Z1683225090	0.879	1.542	1.542	AAAHR_8	A(5) A(6) A(2) H(10) R(14)	0.581	0.694
Z1890693512	0.691	1.540	1.540	AAAHR_6	A(4) A(1) A(3) H(8) R(13)	0.361	0.755
PV-002558797812	0.569	1.775	1.775	AAAHR_6	A(1) A(4) A(3) H(10) R(11)	0.441	0.807
PV-000250468827	0.727	1.619	1.619	AAHHR_1	A(1) A(3) H(6) H(9) R(10)	0.325	0.900
Z1684534882	0.971	1.507	1.507	AAAHR_7	A(4) A(7) A(1) H(9) R(14)	0.524	0.792
PV-000185178177	0.574	1.512	1.512	AAAHR_8	A(1) A(2) A(3) H(7) R(11)	0.342	0.649
PV-001434258746	0.925	1.682	1.682	AAHHR_1	A(1) A(3) H(6) H(8) R(9)	0.568	0.885

Table 12. 2D structures of the 20 hits obtained.

PV-001434258746   PV-002427431755   Z2150792351   Z1683225090

Z1890693512   PV-002558797812   PV-000250468827   Z1684534882

PV-000185178177   PV-002201035475   PV-002215946839   PV-002569833477

Continued

PV-002109864487 PV-001946374534 PV-002493365265 PV-002273233325

Z1683786797 Z2700704516 Z1683053210 Z1694049401
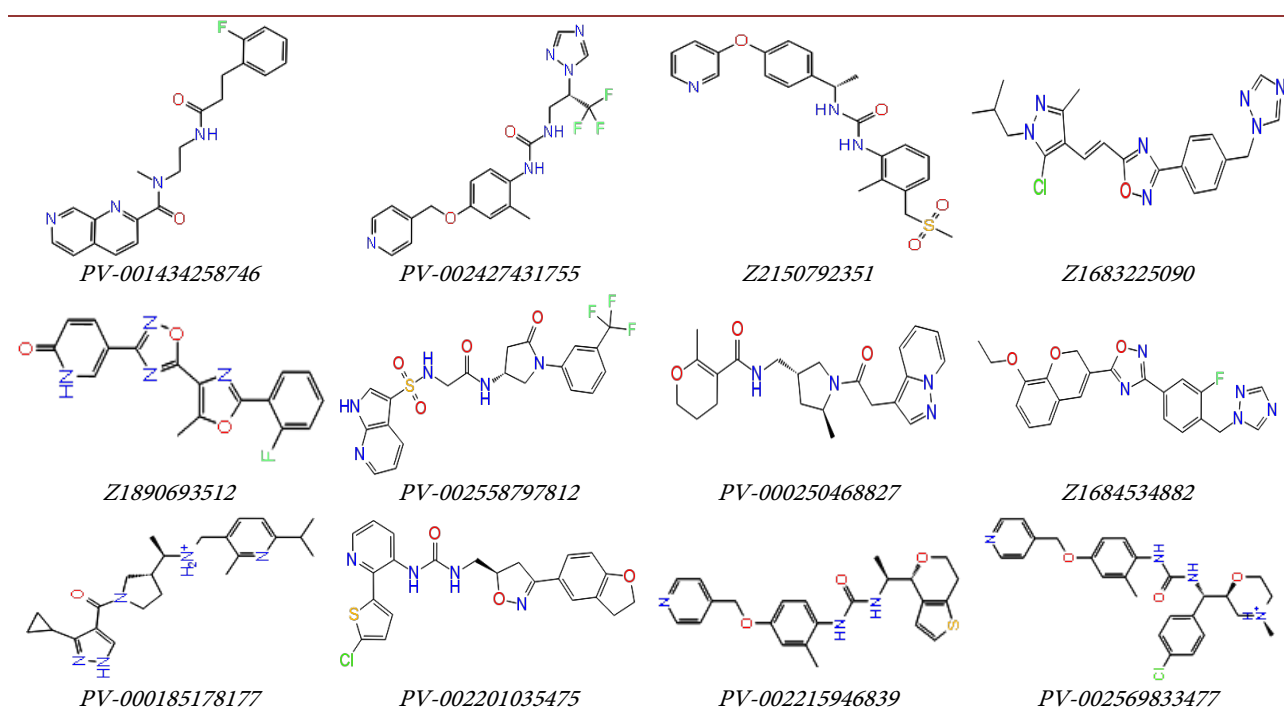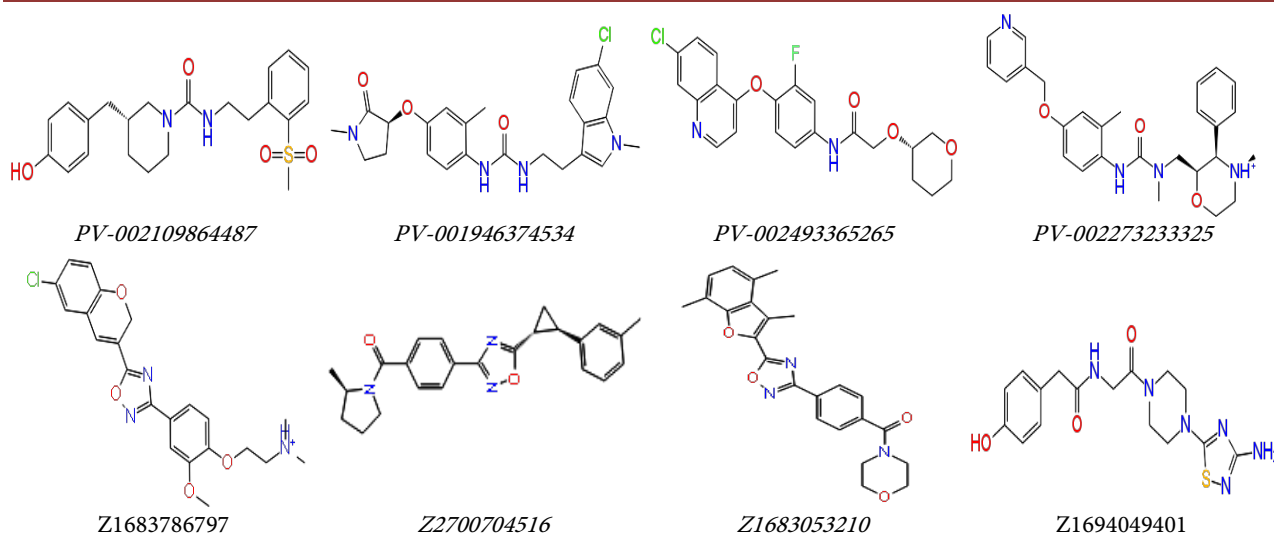
3.7. HTVS, SP and XP Analysis of Hits

The compounds were subjected to a three-stage docking strategy based on Glide in which all compounds were docked through three stages of the docking protocol, high-throughput virtual screening (HTVS), standard precision (SP) and extra precision (XP). In the first step, the Glide high-throughput virtual screening mode was used and 10% of the best performing ligands were used for the next step, Glide SP. Again, 10% of the best performing leads from Glide SP were retained and docked with Glide XP to refine the correct ligands. The glide energy, glide emodel and docking score parameters of HTVS, SP and XP of the selected hits are given in Table 13.

The compounds obtained by XP screening are classified according to the calculated docking score. These values range from −12.031 kcal/mol to −10.959 kcal/mol. These values are all higher than those of the reference molecule. This means that these 20 hits have an affinity comparable to that of the reference molecule, which confers a better stability in the active site of the 3HVE protein.

3.8. Prime MM-GBSA Hits Analysis

The Prime/MM-GBSA method [40] based on the complex obtained after Docking XP was used to calculate the free enthalpy of binding ΔG_{bind} of ligands in the active site of the target protein and the results obtained are summarised in Table 14. The free enthalpy of binding ΔG_{bind} of the hits ranged from −94.520 to −48.197 kcal/mol. All the obtained hits except the compounds Z1683225090 and PV-002569833477 have a binding energy higher than that of the reference ligand.

Van der Waals interactions ΔG_{vdW}, (ranging from −65.383 to −38.016 kcal/mol), electrostatic or coulomb interactions $\Delta G_{coulomb}$ (ranging from -30.244 to −3.18 kcal/mol) and lipophilic interactions ΔG_{lipo} (ranging from −34.648 to −19.472 kcal/mol) are the main energetic factors favorable to ligand binding.

Table 13. Glide energy, glide emodel and docking score of the 20 poses after HTVS, SP and XP screening.

Code of the selected molecules	XP DOCKING			SP DOCKING			HTVS DOCKING		
	GLIDE ENERGY	GLIDE EMODEL	DOCKING SCORE	GLIDE ENERGY	GLIDE EMODEL	DOCKING SCORE	GLIDE ENERGY	GLIDE EMODEL	DOCKING SCORE
Z1890693512	−53.121	−79.763	−12.861	−53.366	−83.231	−10.616	−39.288	−49.569	−7.941
Z2121011596	−58.151	−86.538	−12.840	−52.043	−81.762	−6.906	−51.617	−77.168	−8.035
Z1683225090	−64.298	−103.137	−12.433	−64.844	−110.359	−12.115	67.242	−111.186	−11.339
PV-000185178177	−57.644	−69.817	−12.371	−57.705	−89.764	−10.861	−51.375	−79.966	−8.592
PV-002342843731	−63.185	−83.969	−12.329	−59.201	−99.536	−10.225	−33.959	43.623	−8.925
PV-000250468827	−54.193	−71.666	−12.107	−50.948	−75.131	−10.153	−37.792	−43.805	−8.734
Z1684534882	−63.578	−99.410	−11.819	−61.623	−99.217	−11.478	−36.743	−44.636	−8.603
PV-002558797812	−60.576	−86.861	−11.751	−56.230	−82.206	−8.574	−43.561	−59.921	−8.688
PV-001434258746	−61.101	−90.189	−11.658	−59.853	−92.134	−10.332	−53.774	−79.920	−9.848
PV-002089512142	−62.392	−93.748	−11.583	−51.203	−72.937	−8.309	−51.155	−75.676	−9.663
PV-002569833477	−72.930	−118.200	−13.244	−71.405	−127.462	−12.340	−53.947	79.698	−9.003
PV-002215946839	−65.001	−100.234	−13.146	−66.509	−110.293	−11.323	−61.093	−99.204	−11.020
PV-002201035475	−62.517	−101.253	−12.608	−60.098	−96.858	−10.112	−60.830	−95.374	−9.365
PV-002109864487	−59.216	−85.612	−12.563	−58.314	−91.135	−11.565	−54.752	−82.895	−9.318
PV-002273233325	−65.498	−102.751	−12.552	−65.641	−99.792	−11.689	−51.223	−75.193	−8.708
PV-002427431755	−63.541	−100.593	−12.477	−59.908	−96.100	−10.085	−61.221	−98.663	−10.616
Z1694049401	−55.968	−96.550	−12.402	−61.514	−95.298	−10.186	−56.911	−84.543	−9.115
PV-001946374534	−66.301	−100.558	−12.299	−61.426	−88.396	−10.764	−53.904	−79.556	−10.549
Z1683053210	−55.537	−85.113	−12.096	−57.437	−85.511	−11.977	−44.470	−63.286	−10.419
Z2150792351	−67.718	−97.576	−11.969	−64.079	−100.724	−10.809	−56.062	−86.036	−10.231
Reference molecule	−74.301	−135.427	−14.359	−74.179	−136.033	−14.053	−70.627	−129.068	−13.542

Table 14. Calculated free binding energies (kcal/mol) of the 20 selected molecules.

Code of the selected molecules	ΔG_{bind}	$\Delta G_{coulomb}$	$\Delta G_{covcovalent}$	$\Delta G_{H\text{-}bond}$	ΔG_{lipo}	$\Delta G_{packing}$	ΔG_{solvGB}	ΔG_{vdW}
Z1890693512	−64.031	−19.105	6.796	−1.668	−20.610	−0.506	22.710	−51.649
Z2121011596	−66.083	−29.670	5.501	−2.618	−27.380	−1.207	39.058	−49.767
Z1683225090	−80.346	−14.367	6.374	−1.072	−29.387	−0.626	26.056	−67.323
PV-000185178177	−61.825	−4.454	11.882	−2.264	−30.651	−0.131	21.515	−57.722
PV-002342843731	−74.626	15.358	13.702	−2.145	−34.099	−0.238	−17.971	−49.232
PV-000250468827	−48.110	−27.027	14.730	−1.578	−27.002	−0.028	34.147	−41.352
Z1684534882	−75.065	−17.252	10.419	−1.068	−28.439	−0.589	22.146	−60.282
PV-002558797812	−61.486	−21.019	7.806	−1.643	−17.900	−0.018	31.151	−59.863
PV-001434258746	−73.056	−24.383	4.362	−1.692	−25.925	−1.215	31.476	−55.680
PV-002089512142	−73.521	−29.286	5.833	−3.239	−26.168	−0.221	41.002	−61.442
PV-002569833477	−94.520	−19.812	8.545	−2.215	−35.537	−0.073	24.636	−70.064

Continued

PV-002215946839	−77.154	−27.443	16.497	−2.346	−35.972	−0.850	28.988	−56.027
PV-002201035475	−73.065	−17.419	5.453	−2.382	−31.058	−0.435	33.126	−60.351
PV-002109864487	−57.071	−2.532	17.349	−2.059	−27.254	−0.599	12.194	−54.171
PV-002273233325	−60.892	−22.389	21.837	−1.745	−34.165	−0.869	21.375	−44.935
PV-002427431755	−68.082	−22.639	13.202	−2.363	−25.698	−0.713	28.078	−57.949
Z1694049401	−58.115	−21.128	4.240	−2.852	−18.037	−0.769	34.983	−54.551
PV-001946374534	−74.393	−20.681	11.155	−2.037	−32.117	−1.932	29.550	−58.333
Z1683053210	−70.718	−13.407	11.306	−1.186	−28.349	−1.654	25.542	−62.969
Z2150792351	−70.989	−17.451	9.348	−2.162	−31.546	−0.506	32.147	−60.818
Reference molecule	−79.851	−20.755	2.834	−1.855	−21.190	−0.329	24.626	−63.185

All reported energies are in kilocalories per mole (kcal/mol). ΔG_{bind} free energy of protein−ligand binding; ΔG_{Coul} the columbic binding free energy; ΔG_{Cov} the covalent binding free energy; ΔG_{vdW} van der Waals binding free energy; ΔG_{SolvSA} solvation binding free energy of the surface area; ΔG_{SolvGB} generalized Born solvation binding free energy.

The contribution of hydrogen bonding energy $\Delta G_{\text{H-bond}}$ (ranging from −2.37 to −0.566 kcal/mol) and packing energy $\Delta G_{\text{packing}}$ (ranging from −10.973 to −0.305 kcal/mol) is small in the free enthalpy of binding.

The unfavourable energy contributions to ligand binding are the covalent interaction energy $\Delta G_{\text{covalent}}$ (ranging from 2.566 to 18.012 kcal/mol) and solvation energy ΔG_{solvGB} (ranging from 7.002 to 42.109 kcal/mol).

These results confirm that the molecules obtained have a higher affinity and therefore a possibly higher inhibition rate than the available reference molecule.

3.9. IFD Hits Analysis

The parameters glide energy, glide Emodel, docking score and IFD score as well as the different types of interactions between the hits obtained and the residues of the active site of the 3VHE protein are summarised in Table 15. The docking score, IFD score, glide Emodel, glide energy parameters of the hits obtained are between −14.07 and −10.813 kcal/mol; −645.847 and −617.2 kcal/mol; −123.445 and −71.983 kcal; −73.135 and −50.605 kcal/mol respectively. The binding modes of the new molecules with the lowest IFDscore (Z1694049401) as well as the one with the highest IFDscore (Z1683053210, PV-001434258746) were discussed in detail.

- Binding Mode of Compound Z1683053210

Of all the compounds selected, the compound Z1683053210 was the best inhibitor in this screening with an IFDscore of −632.286 kcal/mol. Visual analysis shows that this compound forms 2 hydrogen bonds with the active site, one of which is with the Asp 1046 residue and the nitrogen of the 1,2,4-oxadiazole ring with a distance of 2.20 Å and an angle $\angle$NHN = 164.7°. The second bond is established between the hydrogen of residue CYS 919 and the oxygen of the morpholine ring with a distance of 1.70 Å and an angle $\angle$NHO = 164°. The LYS 868

Table 15. IFD analysis of the 20 selected molecules.

Code of the selected molecules	glide energy	glide emodel	docking score	IFD score	Hydrogen Bond Interaction	Hydrophobic interaction	Pi-Pi. Pi-Cation. Salt Bridge Interaction
Z2121011596	−65.577	−103.426	−14.657	−639.643	Glu 885, Phe 918, Cys 919, Asp 1046	Leu 840, Val 848, Ala 866, Leu 889, Val 898, Val 899, Val 916, Cys 919, Leu 1019, Leu 1035, Ile 1044, Cys 1045, Phe 1047	Phe 1047
PV-002089512142	−68.303	−107.062	−12.975	−638.221	Glu 885, Cys 919, Asp 1046	Leu 840, Val 848, Ala 866, Ile 888, Leu 889, Val 898, Val 899, Val 916, Cys 919, Leu 1019, Leu 1035, Cys 1045, Phe 1047, Val 916	Phe 1047
PV-002342843731	−73.504	−114.834	−14.133	−637.954	Glu 885, Asp 1046	Leu 840, Val 848, Val 898, Val 899, Val 914, Phe 918, Cys 919, Leu 1019, Leu 1035, Ile 1044, Cys 1045, Phe 1047	Hie 1026. Asp 1046. Phe 1047
Z1683225090	−57.998	−96.381	−14.095	−637.185	Cys 919, Asp 1046	Val 848, Ala 866, Ile 888, Leu 889, Val 898, Val 899, Val 916, Cys 919, Leu 1019, Leu 1035, Ile 1044, Cys 1045, Phe 1047	Lys 868 Phe 1047
Z1890693512	−56.527	−91.994	−14.509	−636.925	Glu 917, Cys 919 Asp 1046	Leu 840, Val 848, Ala 866, Ile 888, Leu 889, Val 899, Val 914, Val 916, Leu 1035, Phe 1047	Lys 868 Phe 1047
PV-002558797812	−66.936	−91.402	−12.247	−636.705	Glu 917 Asp 1046	Val 848, Ile 888, Leu 889, Ile 892, Val 899, Val 916, Leu 1019, Cys 1024, Leu 1035, Phe 1047	Hie 1026 Phe 1047
PV-000250468827	−56.840	−67.676	−11.254	−635.412	Leu 840, Asp 923, Asp 1046	Leu 840, Val 848, Ala 866, Val 899, Val 916, Cys 919, Phe 1047	Phe 1047
Z1684534882	−62.921	−96.818	−13.148	−634.956	Cys 919 Asp 1046	Leu 840, Val 848, Ala 866, Ile 888, Leu 889, Ile 892, Phe 918, Cys 919, Leu 1019, Cys 1024, Leu 1035, Cys 1045, Phe 1047	Lys 868 Hie 1026 Phe 1047
PV-000185178177	−44.945	−72.693	−11.632	−634.761	Glu 885	Val 848, Ala 866, Ile 888, Leu 889, Ile 892, Val 899, Val 914, Val 916, Phe 918, Cys 919, Leu 1019, Leu 1035, Cys 1045, Phe 1047	Phe 1047
PV-001434258746	−63.550	−98.254	−13.267	−633.864	Glu 885 Asp 1046 Cys 919	Leu 840, Val 848, Ala 866, Leu 889, Val 916, Phe 918, Cys 919, Leu 1019, Leu 1035, Ile 1044, Cys 1045, Phe 1047	Hie 1026 Phe 1047
Z1694049401	−64.246	−111.153	−12.961	−640.905	Cys 919, Cys 1045, Asp 1046 Glu 885	Val 848, Ala 866, Leu 889, Ile 892, Val 898, Val 899, Val 916, Leu 1035, Ile 1044, Cys 1045, Phe 1047	…

Continued

Z2150792351	−72.672	−117.600	−13.461	−639.538	GLU 885 ASP 1046	Leu 840, Val 848, Ala 866, Ile 888, Leu 889, Ile 892, Val 898, Val 899, Phe 918, Leu 1019, Leu 1035, Cys 1045, Phe 1047	Phe 1047
PV-002427431755	−64.845	−105.371	−14.555	−638.659	Glu 885, Asp 1046 Cys 919, Cys 1045	Leu 840, Val 848, Ala 866, Leu 889, Val 914, Val 916, Phe 918, Cys 919, Leu 1035, Cys 1045, Phe 1047	Hie 1026
PV-002201035475	−68.464	−115.225	−13.511	−638.470	Cys 919, Cys 1045, Glu 885	Leu 840, Val 848, Ala 866, Val 916, Phe 918, Cys 919, Leu 1035, Ile 1044, Phe 1047	Hie 1026
PV-002215946839	−72.513	−123.582	−14.122	−638.400	Cys 919, Cys 1045, Glu 885	Leu 840, Val 848, Ala 866, Leu 889, Val 916, Cys 919, Leu 1035, Cys 1045, Phe 1047	Phe 1047
PV-002569833477	−76.404	−129.232	−14.065	−637.902	Asp 1046 Cys 919 Glu 885	Leu 840, Val 848, Ala 866, Ile 888, Leu 889, Ile 892, Val 898, Val 899, Val 914, Val 916, Phe 918, Cys 919, Leu 1019, Leu 1035, Ile 1044, Cys 1045, Phe 1047	Lys 868
PV-002109864487	−64.889	−104.365	−13.489	−637.822	Asp 1046 Cys 919 Glu 885	Leu 840, Val 848, Ala 866, Leu 889, Val 899, Val 916, Cys 919, Leu 1019, Ile 1044, Cys 1045, Phe 1047	Hie 1026
PV-001946374534	−73.791	−119.661	−13.759	−637.524	GLU 885 Asp 1046 Cys 919	Leu 840, Val 848, Ala 866, Ile 888, Leu 889, Ile 892, Val 899, Val 914, Val 916, Phe 918, Leu 1019, Leu 1035, Cys 1045, Phe 1047	Hie 1026
PV-002273233325	−67.973	−113.097	−13.057	−635.841	Glu 885 Cys 919	Leu 840, Val 848, Ala 866, Ile 888, Leu 889, Ile 892, Val 896, Val 899, Val 916, Phe 918, Cys 919, Leu 1019, Leu 1035 Ile 1044, Cys 1045, Phe 1047	Hie 1026. Asp 1046. Phe 1047
Z1683053210	−51.809	−92.257	−13.859	−632.286	Asp 1046 Cys 919	Leu 840, Val 848, Ala 866, Ile 888, Leu 889, Ile 892, Val 899, Val 916, Phe 918, Cys 919, Leu 1035, Ile 1044, Cys 1045, Phe 1047	Lys 868 Hie 1026 Phe 1047
Reference molecule	−66.050	−113.417	−12.946	−637.884	Glu 885 Cys 919 Asp 1046	Leu 840, Val 848, Ala 866, Lys 868, Glu 885, Ile 888, Leu 889, Ile 892, Val 898, Val 899, Val 916, Glu 917, Phe 918, Cys 919, Glu 922, Hie 1026, Leu 1035, Ile 1044, Cys 1045, Asp 1046, Phe 1047	…

residue engages in a pi-cation bond with the morpholine ring. The benzene group and benzofuran of the compound establish π-π bonds with the Phe 1047

and Hie 1026 residue respectively. Finally, this compound establishes a pi-cation bond with the residue Lys 868 (Figure 7).

Numerous hydrophobic interactions also ensure the stability of the 3VHE-PV-001434258746 complex. These interactions are found between the inhibitor and residues Leu 840, Val 848, Ala 866, Leu 889, Val 916, Phe 918, Cys 919, Leu 1019, Leu 1035, Ile 1044, Cys 1045 and Phe 1047 (Figure 8).

- Binding mode of the compound PV-001434258746

The compound PV-001434258746 is considered the second best inhibitor that came out of our virtual screening with an IFDscore of −633.864 kcal/mol. It establishes three hydrogen bonds with the 3VHE receptor. A first bond between the hydrogen of residue Asp1046 and the oxygen of the carbonyl group with a distance of 1.98 Å and an angle $\angle NHO = 149.7°$. A second bond is established between the hydrogen of residue Cys919 and the 1,7-naphthyridine nitrogen with a distance of 2.12 Å and an angle $\angle NHN = 147.8°$. The last bond is observed between the hydrogen of the nitrogen near the carbonyl group and the oxygen of residue VAL 916 with a distance of 1.78 Å and an angle $\angle NHO = 141.5°$. This compound establishes two π-π bonds between its benzene ring and the Hie 1026 residue and then between the 1,7-naphthyridine and the Phe 1047 residue (Figure 9).

Numerous hydrophobic-type interactions also ensure the stability of the 3VHE-PV-001434258746 complex. These interactions are observed between the inhibitor and the residues Leu 840, Val 848, Ala 866, Leu 889, Val 916, Phe 918, Cys 919, Leu 1019, Leu 1035, Ile 1044, Cys 1045 and Phe 1047 (Figure 10).

Figure 7. Binding mode of compound Z1683053210 in the active site cavity of the 3VHE receptor.
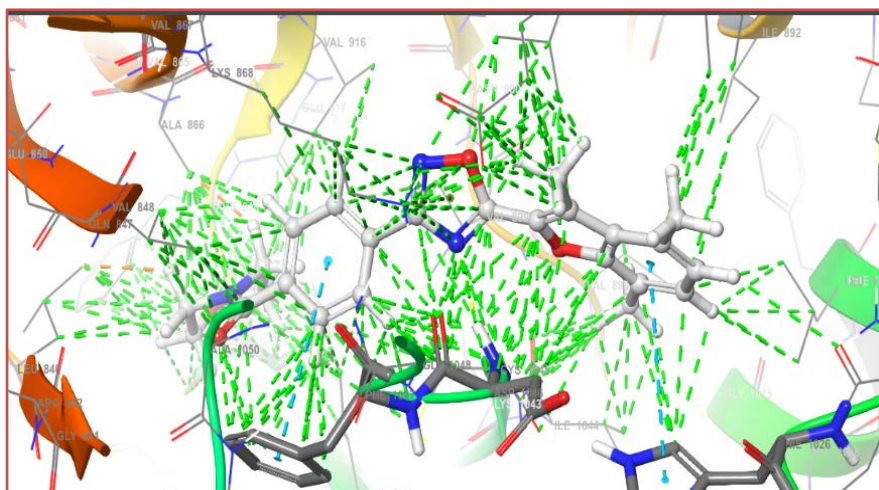
Figure 8. Hydrophobic interactions (green color) of the Z1683053210 compound with the active site residue of 3VHE.
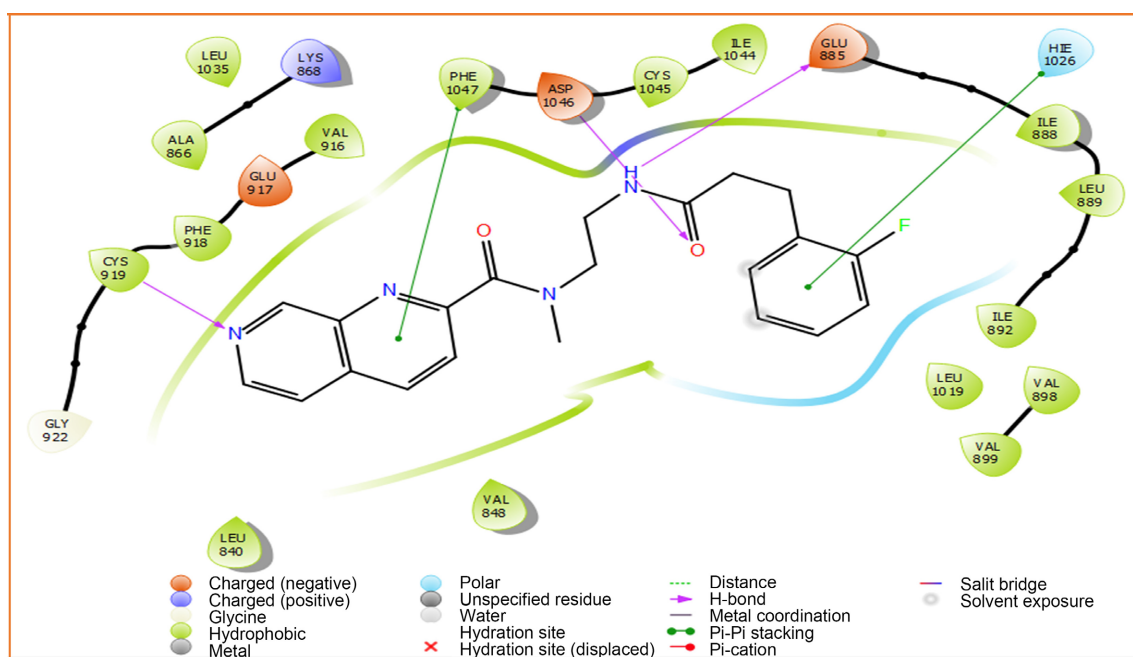
Figure 9. Binding mode of compound PV-001434258746 in the active site cavity of the 3VHE receptor.

- Binding mode of compound Z1694049401

Z1694049401 establishes six hydrogen bonds with the 3VHE receptor. Through its two oxygen atoms in its two carbonyl groups, it establishes two hydrogen bonds with residue ASP 1046 with distances of 1.97 Å and 2.52 Å making angles ∠NHO equal to 128.8° and 158.5°. The hydrogen of residue CYS 1045 establishes a third hydrogen bond with the oxygen of one of the carboxylic functions with a distance d (H...N) = 2.64 Å and an angle ∠SHO = 123.3°. Cys residue 919 also establishes two hydrogen bonds, one of which is with the nitrogen of the 1,2,4-thiadiazole and the other with the hydrogen of the nitrogen close to this group with distances of 2.09 Å and 2 Å, respectively. These bonds are made with

Figure 10. Hydrophobic interactions (green color) of PV-001434258746 with residues of the 3VHE active site.

angles $\angle NHN = 151.6°$ and $\angle NHO = 151.8°$, respectively. The last bond involves the oxygen of the Glu 885 residue and the hydrogen of the nitrogen located between the two carboxylic functions with a distance of 1.69 Å and an angle $\angle NHN = 162.5°$ (**Figure 11**).

It is also necessary to underline the intervention of residues Val 848, Ala 866, Leu 889, Ile 892, Val 898, Val 899, Val 916, Leu 1035, Ile 1044, Cys 1045 and Phe 1047 in the stability of the 3VHE-Z1694049401 complex by the formation of numerous hydrophobic interactions between these residues and the compound Z1694049401 (**Figure 12**).

3.10. Prediction of Hit Activity

The 3D-QSAR model constructed above was used to predict the inhibitory activity of the twenty molecules (20) selected after virtual screening. The predicted IC50 activity (µM) of the twenty molecules (20) varies between 0.408 µM and 0.817 µM (**Table 16**). These theoretical activities calculated for the new molecules obtained after virtual screening are significantly lower than that obtained by Coulibaly *et al.* [15] (between 0.587 µM and 0.756 µM). These new compounds show better or similar biological activities to those of the molecules synthesized by Coulibaly *et al.* [15]. These molecules could constitute a solid basis in the search for new inhibitors of 3VHE prostate cancer cells.

3.11. ADMET Properties of New Compounds

The ADMET properties of the 20 newly identified hits were evaluated using Qikprop. The results obtained are reported in **Table 17**. The above 20 hits meet the drug properties based on Lipinski's rule five. The pharmacokinetic parameters (ADME-Tox) for all 20 hits are within an acceptable range for human use, revealing their potential drug-like properties.

QPlogPo/w is the expected octanol/water partition coefficient; QPlogS predicts the solubility in water. log S. S in mol/l is the concentration of the solute in
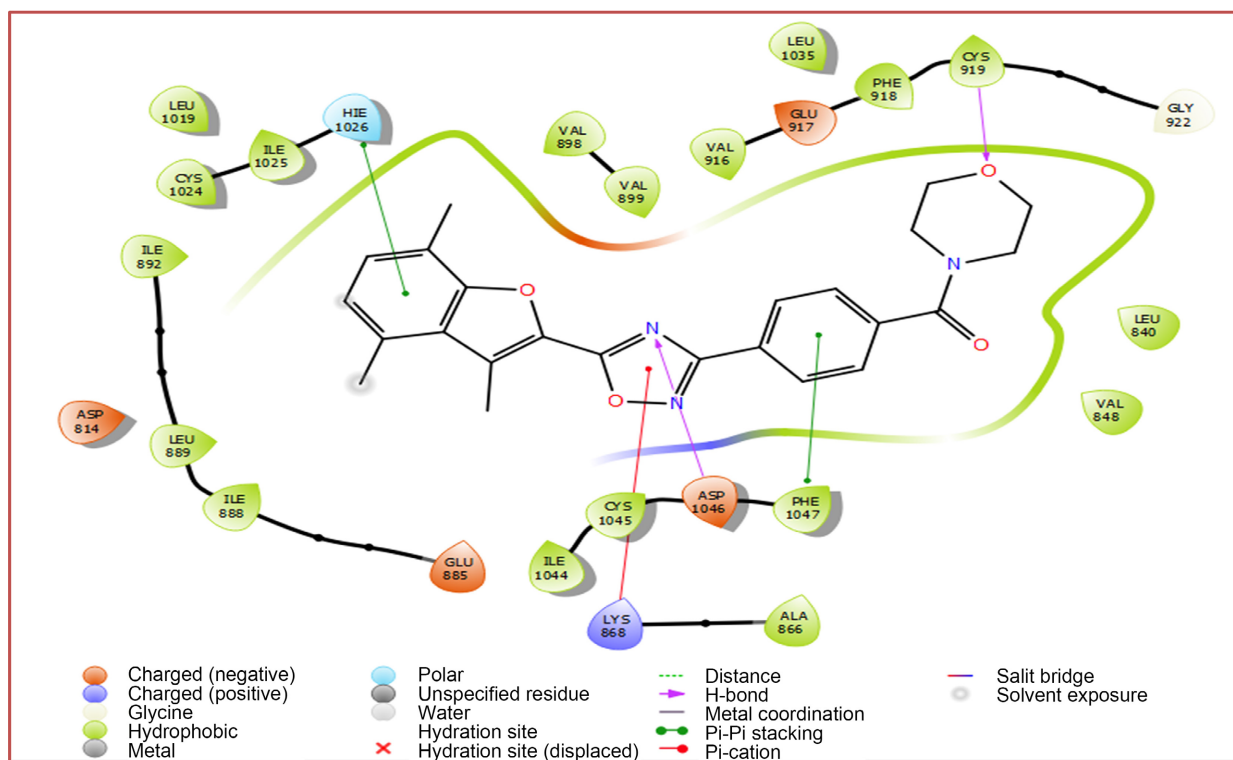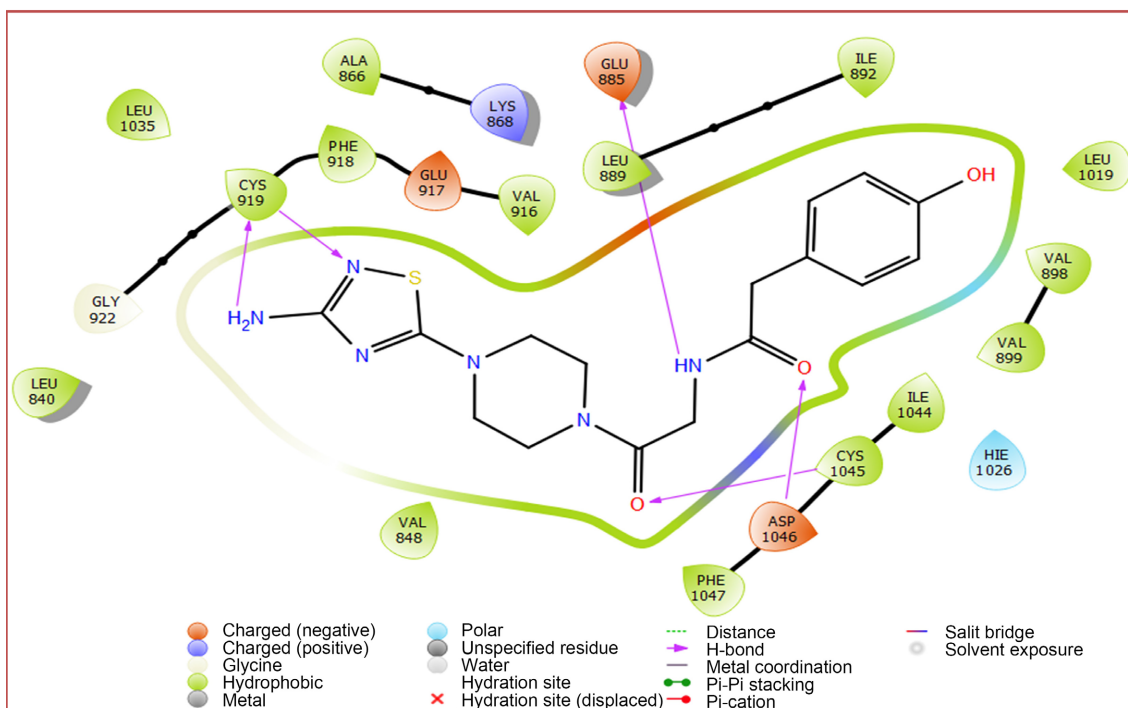
Figure 11. Binding mode of compound Z1694049401 in the active site cavity of the 3VHE receptor.

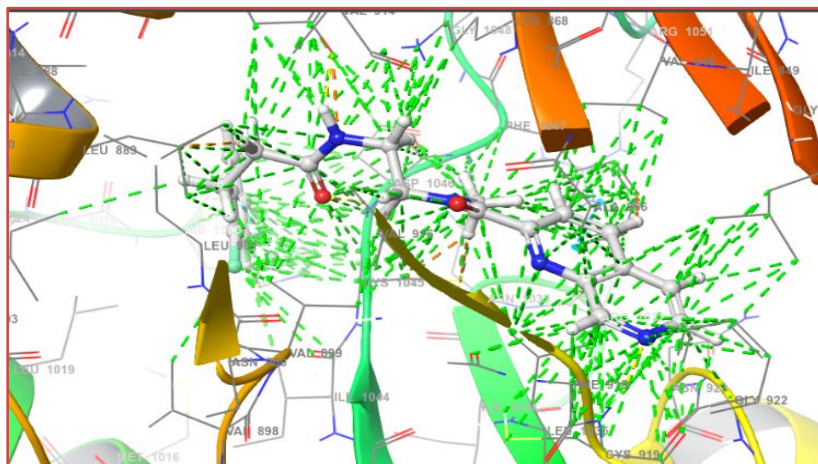**Figure 12.** Hydrophobic interactions of Z1694049401 with residues of the 3VHE active site.

Table 16. Predicted activities of new molecules.

Code of the selected molecules	PIC$_{50}$	IC$_{50}$
PV-002089512142	4.126	0.748
PV-002342843731	4.141	0.723
PV-001894667629	4.197	0.635
Z1683225090	4.091	0.811
Z1890693512	4.162	0.689

Continued

PV-002558797812	4.219	0.604
PV-000250468827	4.313	0.486
Z1684534882	4.166	0.682
PV-000185178177	4.389	0.408
PV-001434258746	4.123	0.753
Z1694049401	4.223	0.598
Z2150792351	4.230	0.589
PV-002427431755	4.158	0.695
PV-002201035475	4.196	0.637
PV-002215946839	4.223	0.598
PV-002569833477	4.268	0.539
PV-002109864487	4.162	0.688
PV-001946374534	4.102	0.791
PV-002493365265	4.088	0.817
PV-002273233325	4.106	0.783
Z1683786797	4.090	0.813
Z2700704516	4.186	0.651
Z1683053210	4.111	0.774

Table 17. ADMET properties of the 20 new compounds.

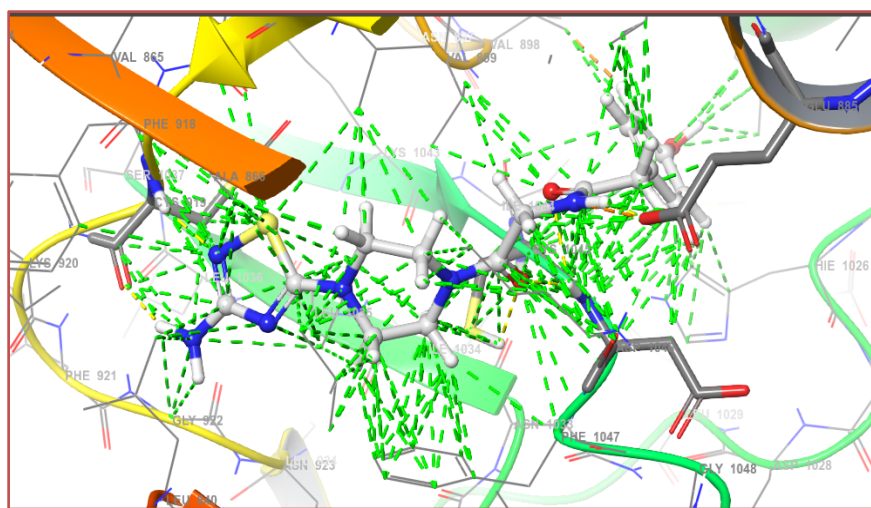| Code of the selected molecules	QPlogS	QPPCaco	Rule Of Three	QPlog BB	QPlogK hsa	Mol MW	PSA	Percent Human Oral Absorption	QPPMDCK	QPlogPo/w
PV-002089512142	−3.743	127.570	0	−1.607	−0.512	384.434	116.049	73.876	131.752	1.578
PV-002342843731	−5.818	632.259	2	−1.277	0.162	423.514	97.196	100.000	389.581	3.676
PV-001894667629	−5.032	475.852	0	−0.870	0.182	364.335	101.092	91.631	320.696	2.863
Z1683225090	−6.298	599.087	1	−1.209	0.393	423.904	84.584	100.000	503.773	4.356
Z1890693512	−4.671	360.507	0	−0.875	−0.073	338.297	99.722	84.507	252.848	2.015
PV-002558797812	−5.331	32.887	0	−2.099	−0.163	481.449	146.586	67.314	104.958	2.257
PV-000250468827	−6.194	977.227	1	−0.771	0.282	396.488	88.471	100.000	706.900	3.685
Z1684534882	−5.759	1004.855	1	−0.768	0.157	419.414	84.093	100.000	749.829	3.820
PV-000185178177	−5.673	268.889	0	−0.489	0.921	395.547	78.514	95.759	132.332	4.326
PV-001434258746	−3.815	444.498	0	−1.001	−0.296	380.421	88.439	89.521	515.655	2.593
Z1694049401	−2.990	20.953	1	−2.242	−0.871	376.432	145.013	50.775	34.479	0.031
Z2150792351	−5.520	366.131	0	−1.332	0.150	439.528	102.345	92.663	251.897	3.387
PV-002427431755	−5.487	466.498	0	−0.957	−0.015	420.393	95.953	94.649	1215.369	3.405
PV-002201035475	−4.660	1052.444	0	−0.303	0.246	454.930	87.020	100.000	1191.194	3.431
PV-002215946839	−6.588	1082.971	2	−0.597	0.520	423.529	73.381	100.000	1652.810	4.619

Continued

PV-002569833477	−6.109	349.388	2	−0.148	0.506	480.993	79.077	100.000	652.994	4.455
PV-002109864487	−5.250	176.381	0	−1.594	0.264	416.534	96.093	86.557	133.007	3.314
PV-001946374534	−4.286	426.432	0	−0.615	0.227	454.955	83.148	95.352	1049.505	3.644
PV-002493365265	−5.784	2568.446	1	−0.171	0.292	430.862	70.439	100.000	5469.819	4.363
PV-002273233325	−2.495	464.206	1	0.123	0.173	460.575	63.279	93.601	386.392	3.232
Z1683786797	−5.158	743.832	0	0.208	0.306	427.886	65.549	100.000	981.167	4.079
Z2700704516	−7.200	1442.726	1	−0.480	0.815	387.480	67.018	100.000	735.206	4.718
Z1683053210	−5.516	1289.640	0	−0.484	0.160	417.463	82.780	100.000	651.259	3.429

a saturated solution which is in equilibrium with the crystalline solid; QPPCaco predicted the apparent permeability of Caco-2 cells in nm/sec; Caco-2 cells are a model for the intestinal blood barrier; QPPMDCK Expected apparent permeability of MDCK cells in nm/sec; QPlogBB predicted brain/blood partition coefficient.

[Recommended values]: PSA = 7 to 200; QPPCaCo < 25 Poor, >500 Good; QPPMDCK < 25 Poor; >500 Excellent; QlogBB between −3.0 and −1.2; QPlogPo/w between −2 and 6.5; QPlogS between −6.5 and 0.5; QPlogKhsa between −1.5 and 1.5; MW between 130 and 725.

4. Conclusion

In this study, a pharmacophore modeling and virtual screening protocol was performed to identify novel prostate cancer inhibitors. Using *in vitro* data of prostate cancer inhibitors, we constructed different pharmacophore hypotheses using PHASE software. In addition, the discriminatory ability of the pharmacophore models was validated by enrichment studies using the DECOY method. The developed models show significant value of validation parameters AUC, ROC, BEDROC and RIE. The obtained pharmacophore models were used to screen a set of molecules from the Enamine database. We also developed an atom-based 3D-QSAR model using 56 molecules in the test set and 18 molecules in the validation set. The generated model exhibited a high coefficient of determination (R^2 = 0.9032) and cross-validation coefficient (Q^2 = 0.8695) with low RMSE (0.08) and SD (0.0813). The high predictive ability of this model was validated by an external validation test on all molecules in the validation set. Analysis of the atom-based 3D-QSAR contour representation revealed the structural requirements to enhance the biological activity of the inhibitors against the prostate cancer enzyme. Compounds selected by the VSW protocol were subjected to free enthalpy of binding calculation by the Prime-MMGBSA protocol, IFD: induced fit docking protocol, and pharmacological properties calculation (ADMET). The results suggest that all the 20 hits obtained satisfy good in silico criteria such as Docking score, ADME properties, presence of hydrogen bonding interaction and also favorable and lower binding energy and IFD score than the reference molecule.

Conflicts of Interest

The authors declare no conflicts of interest regarding the publication of this paper.

References

[1] Parkin, D., Bray, F. and Devesa, S. (2001) Cancer Burden in the Year 2000. The Global Picture. *European Journal of Cancer*, **37**, 466.
https://doi.org/10.1016/S0959-8049(01)00267-2

[2] Jeong, T.-S., Kim, J.-R., Kim, K.S., Cho, K.-H., Bae, K.-H. and Lee, W.S. (2004) Inhibitory Effects of Multi-Substituted Benzylidenethiazolidine-2, 4-Diones on LDL Oxidation. *Bioorganic & Medicinal Chemistry*, **12**, 4017-4023.
https://doi.org/10.1016/j.bmc.2004.06.001

[3] Koppireddi, S., Komsani, J.R., Avula, S., Pombala, S., Vasamsetti, S., Kotamraju, S. and Yadla, R. (2013) Novel 2-(2,4-dioxo-1,3-thiazolidin-5-yl) Acetamides as Antioxidant and/or Anti-Inflammatory Compounds. *European Journal of Medicinal chemistry*, **66**, 305-313. https://doi.org/10.1016/j.ejmech.2013.06.005

[4] Barros, C.D., Amato, A.A., de Oliveira, T.B., Iannini, K.B.R., da Silva, A.L., da Silva, T.G., Leite, E.S., Hernandes, M.Z., de Lima, M.d.C.A. and Galdino, S.L. (2010) Synthesis and Anti-Inflammatory Activity of New Arylidene-Thiazolidine-2,4-Diones as PPARγ Ligands. *Bioorganic & Medicinal Chemistry*, **18**, 3805-3811.
https://doi.org/10.1016/j.bmc.2010.04.045

[5] Heerding, D.A., Christmann, L.T., Clark, T.J., Holmes, D.J., Rittenhouse, S.F., Takata, D.T. and Venslavsky, J.W. (2003) New Benzylidenethiazolidinediones as Antibacterial Agents. *Bioorganic & Medicinal Chemistry Letters*, **13**, 3771-3773.
https://doi.org/10.1016/j.bmcl.2003.07.010

[6] Trotsko, N., Kosikowska, U., Paneth, A., Wujec, M. and Malm, A. (2018) Synthesis and Antibacterial Activity of New (2,4-Dioxothiazolidin-5-yl/ylidene) Acetic Acid Derivatives with Thiazolidine-2,4-Dione, Rhodanine and 2-Thiohydantoin Moieties. *Saudi Pharmaceutical Journal*, **26**, 568-577.
https://doi.org/10.1016/j.jsps.2018.01.016

[7] Marc, G., Ionuţ, I., Pirnau, A., Vlase, L., Vodnar, D.C., Duma, M., Tiperciuc, B. and Oniga, O. (2017) Microwave Assisted Synthesis of 3,5-Disubstituted Thiazolidine-2,4-Diones with Antifungal Activity. Design, Synthesis, Virtual and *in Vitro* Antifungal Screening. *Farmacia*, **65**, 414-422.

[8] Tuncbilek, M. and Altanlar, N. (2006) Synthesis of New 3-(Substituted Phenacyl)-5-[3'-(4H-4-oxo-1-benzopyran-2-yl)-benzylidene]-2,4-Thiazolidinediones and Their Antimicrobial Activity. *Archiv der Pharmazie*, **339**, 213-216.
https://doi.org/10.1002/ardp.200500180

[9] Liu, X.-F., Zheng, C.-J., Sun, L.-P., Liu, X.-K. and Piao, H.-R. (2011) Synthesis of New Chalcone Derivatives Bearing 2, 4-Thiazolidinedione and Benzoic Acid Moieties as Potential Anti-Bacterial Agents. *European Journal of Medicinal Chemistry*, **46**, 3469-3473. https://doi.org/10.1016/j.ejmech.2011.05.012

[10] Ibrahim, M.A., Abdel-Hamed, M.A.-M. and El-Gohary, N.M. (2011) A New Approach for the Synthesis of Bioactive Heteroaryl Thiazolidine-2, 4-Diones. *Journal of the Brazilian Chemical Society*, **22**, 1130-1139.
https://doi.org/10.1590/S0103-50532011000600019

[11] Mousavi, S.M., Zarei, M., Hashemi, S.A., Babapoor, A. and Amani, A.M. (2019) A Conceptual Review of Rhodanine. *Artificial Cells, Nanomedicine, and Biotechnol-*

ogy, **47**, 1132-1148. https://doi.org/10.1080/21691401.2019.1573824

[12] Almeida, V.L.d., Lopes, J.C.D., Oliveira, S.R., Donnici, C.L. and Montanari, C.A. (2010) Estudos de relações estrutura-atividade quantitativas (QSAR) de bis-benza-midinas com atividade antifúngica. *Química Nova*, **33**, 1482-1489. https://doi.org/10.1590/S0100-40422010000700011

[13] Andrade, C.H., Pasqualoto, K.F.M., Ferreira, E.I. and Hopfinger, A.J. (2010) 4D-QSAR. *Molecules*, **15**, 3281-3294. https://doi.org/10.3390/molecules15053281

[14] Cantello, B.C.C., Cawthorne, M.A., Haigh, D., Hindley, R.M., Smith, S.A. and Thurl-by, P.L. (1994) The Synthesis of BRL 49653—A Novel and Potent Antihyperglycae-mic Agent. *Bioorganic & Medicinal Chemistry Letters*, **4**, 1181-1184. https://doi.org/10.1016/S0960-894X(01)80325-5

[15] Coulibaly, W.K., Paquin, L., Bénié, A., Bekro, Y.-A., Durieux, E., Meijer, L., Le Guével, R., Corlu, A. and Bazureau, J.-P. (2012) Synthesis of New *N,N'*-Bis (5-Ary-lidene-4-Oxo-4,5-Dihydrothiazolin-2-Yl) Piperazine Derivatives under Microwave Irradiation and Preliminary Biological Evaluation. *Scientia Pharmaceutica*, **80**, 825-836. https://doi.org/10.3797/scipharm.1206-04

[16] Schrödinger Release 2017-4: LigPrep (2017). Schrödinger, LLC, New York.

[17] Shivakumar, D., Williams, J., Wu, Y., Damm, W., Shelley, J. and Sherman, W. (2010) Prediction of Absolute Solvation Free Energies Using Molecular Dynamics Free Energy Perturbation and the OPLS Force Field. *Journal of Chemical Theory and Computation*, **6**, 1509-1519. https://doi.org/10.1021/ct900587b

[18] Dixon, S.L., Smondyrev, A.M., Knoll, E.H., Rao, S.N., Shaw, D.E. and Friesner, R.A. (2006) PHASE: A New Engine for Pharmacophore Perception, 3D QSAR Model Development, and 3D Database Screening: 1. Methodology and Preliminary Results. *Journal of Computer-Aided Molecular Design*, **20**, 647-671. https://doi.org/10.1007/s10822-006-9087-6

[19] Dixon, S.L., Smondyrev, A.M. and Rao, S.N. (2006) PHASE: A Novel Approach to Pharmacophore Modeling and 3D Database Searching. *Chemical Biology & Drug Design*, **67**, 370-372. https://doi.org/10.1111/j.1747-0285.2006.00384.x

[20] Huang, N., Shoichet, B.K. and Irwin, J.J. (2006) Benchmarking Sets for Molecular Docking. *Journal of Medicinal Chemistry*, **49**, 6789-6801. https://doi.org/10.1021/jm0608356

[21] Mysinger, M.M., Carchia, M., Irwin, J.J. and Shoichet, B.K. (2012) Directory of Useful Decoys, Enhanced (DUD-E). *Journal of Medicinal Chemistry*, **55**, 6582-6594. https://doi.org/10.1021/jm300687e

[22] Schrödinger Release 2017-4: Phase (2017). Schrödinger, LLC, New York.

[23] Braga, R.C. and Andrade, C.H. (2013) Assessing the Performance of 3D Pharma-cophore Models in Virtual Screening. *Current Topics in Medicinal Chemistry*, **13**, 1127-1138. https://doi.org/10.2174/1568026611313090010

[24] Yang, J.M. and Shen, T.W. (2005) A Pharmacophore Based Evolutionary Approach for Screening Selective. *Proteins: Structure, Function, and Bioinformatics*, **59**, 205-220. https://doi.org/10.1002/prot.20387

[25] Teli, M.K. and Rajanikant, G.K. (2012) Pharmacophore Generation and Atom-Based 3D-QSAR of Novel Quinoline-3-Carbonitrile Derivatives as Tpl2 Kinase In-hibitors. *Journal of Enzyme Inhibition and Medicinal Chemistry*, **27**, 558-570. https://doi.org/10.3109/14756366.2011.603128

[26] Prakash Tanwar, O., Karthikeyan, C., Hari Narayana Moorthy, N.S. and Trivedi, P. (2010) 3D QSAR of Aminophenyl Benzamide Derivatives as Histone Deacetylase

Inhibitors. *Medicinal Chemistry*, **6**, 277-285.
https://doi.org/10.2174/157340610793358846

[27] Wang, H., Aslanian, R. and Madison, V.S. (2008) Induced-Fit Docking of Mometasone Furoate and Further Evidence for Glucocorticoid Receptor 17α Pocket Flexibility. *Journal of Molecular Graphics and Modelling*, **27**, 512-521.
https://doi.org/10.1016/j.jmgm.2008.09.002

[28] Saubern, S., Guha, R. and Baell, J.B. (2011) KNIME Workflow to Assess PAINS Filters in SMARTS Format. Comparison of RDKit and Indigo Cheminformatics Libraries. *Molecular Informatics*, **30**, 847-850. https://doi.org/10.1002/minf.201100076

[29] Schrödinger Release 2017-4: QikProp (2017). Schrödinger, LLC, New York.

[30] Samal, S.K., Routray, S., Veeramachaneni, G.K., Dash, R. and Botlagunta, M. (2015) Ketorolac Salt Is a Newly Discovered DDX3 Inhibitor to Treat Oral Cancer. *Scientific Reports*, **5**, Article No. 9982. https://doi.org/10.1038/srep09982

[31] Truchon, J.-F. and Bayly, C.I. (2007) Evaluating Virtual Screening Methods. *Journal of Chemical Information and Modeling*, **47**, 488-508.
https://doi.org/10.1021/ci600426e

[32] Kumar, A., Roy, S., Tripathi, S. and Sharma, A. (2016) Molecular Docking Based Virtual Screening of Natural Compounds as Potential BACE1 Inhibitors. *Journal of Biomolecular Structure and Dynamics*, **34**, 239-249.
https://doi.org/10.1080/07391102.2015.1022603

[33] Imberty, A., Hardman, K.D., Carver, J.P. and Perez, S. (1991) Molecular Modelling of Protein-Carbohydrate Interactions. Docking of Monosaccharides in the Binding Site of Concanavalin A. *Glycobiology*, **1**, 631-642.
https://doi.org/10.1093/glycob/1.6.631

[34] Sindhu, T. and Srinivasan, P. (2014) Pharmacophore Modeling, 3D-QSAR and Molecular Docking Studies of Benzimidazole Derivatives as Potential FXR Agonists. *Journal of Receptor and Signal Transduction Research*, **34**, 241-253.
https://doi.org/10.3109/10799893.2014.885048

[35] Veerasamy, R., Rajak, H., Jain, A., Sivadasan, S., Varghese, C.P. and Agrawal, R.K. (2011) Validation of QSAR Models-Strategies and Importance. *International Journal of Drug Design and Discovery*, **2**, 511-519.

[36] Berman, E. and Machin, S. (2000) Skill-Biased Technology Transfer around the World. *Oxford Review of Economic Policy*, **16**, 12-22.
https://doi.org/10.1093/oxrep/16.3.12

[37] Rask-Andersen, M., Masuram, S. and Schiöth, H.B. (2014) The Druggable Genome. *Annual Review of Pharmacology and Toxicology*, **54**, 9-26.
https://doi.org/10.1146/annurev-pharmtox-011613-135943

[38] Lengauer, T., Lemmen, C., Rarey, M. and Zimmermann, M. (2004) Novel Technologies for Virtual Screening. *Drug discovery today*, **9**, 27-34.
https://doi.org/10.1016/S1359-6446(04)02939-3

[39] Schrödinger Release 2017-4: Glide (2017). Schrödinger, LLC, New York.

[40] Li, H. (2011) A statistical Framework for SNP Calling, Mutation Discovery, Association Mapping and Population Genetical Parameter Estimation from Sequencing Data. *Bioinformatics*, **27**, 2987-2993. https://doi.org/10.1093/bioinformatics/btr509